Journal Pre-proof

Redox imbalance is associated to lung damage triggered by silver nanoparticles exposure

Garcés Mariana, Magnani Natalia D, Pecorelli Alessandra, Calabró Valeria, Marchini Timoteo, Cáceres Lourdes, Pambianchi Erika, Galdoporpora Juan, Vico Tamara, Salgueiro Jimena, Zubillaga Marcela, Moretton Marcela A, Desimone Martin F, Alvarez Silvia, Valacchi Giuseppe, Evelson Pablo

PII: S0891-5849(21)00081-2

DOI: https://doi.org/10.1016/j.freeradbiomed.2021.02.008

Reference: FRB 15071

To appear in: *Free Radical Biology and Medicine*

Received Date: 22 December 2020

Revised Date: 18 January 2021

Accepted Date: 4 February 2021

Please cite this article as: G. Mariana, M. Natalia D, P. Alessandra, C. Valeria, M. Timoteo, C. Lourdes, P. Erika, G. Juan, V. Tamara, S. Jimena, Z. Marcela, M. Marcela A, D. Martin F, A. Silvia, V. Giuseppe, E. Pablo, Redox imbalance is associated to lung damage triggered by silver nanoparticles exposure, *Free Radical Biology and Medicine*, https://doi.org/10.1016/j.freeradbiomed.2021.02.008.

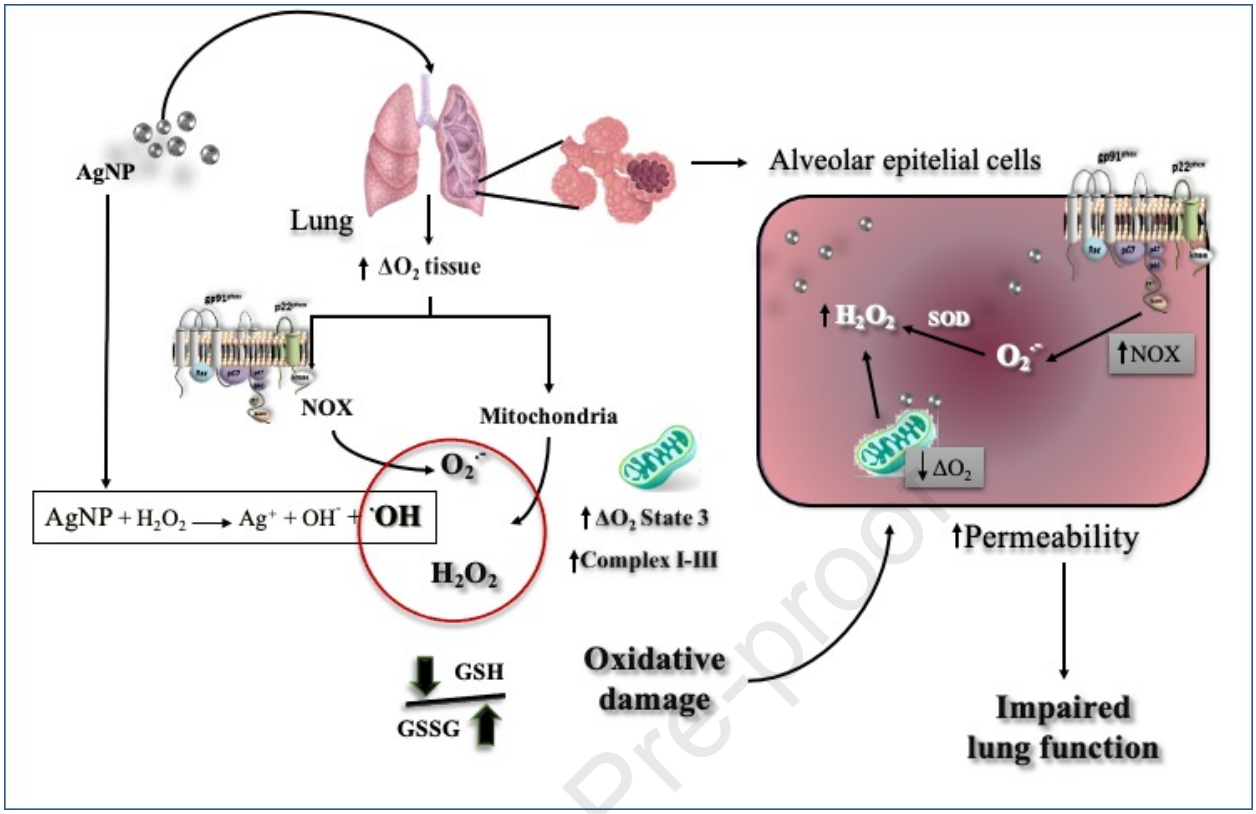

ALTERATIONS IN OXYGEN METABOLISM ARE ASSOCIATED TO LUNG TOXICITY TRIGGERED BY SILVER NANOPARTICLES EXPOSURE

Garcés Mariana[1,2], Magnani Natalia D[1,2], Pecorelli Alessandra[3], Calabró Valeria[1,2], Marchini Timoteo[1,2], Cáceres Lourdes [1,2], Pambianchi Erika[3], Galdoporpora Juan[5,6], Vico Tamara[2,7], Salgueiro Jimena[8], Zubillaga Marcela[8], Moretton Marcela A[9], Desimone Martin F[5,6], Alvarez Silvia[2,7], Valacchi Giuseppe[3,4,10], Evelson Pablo[1,2*].*

[1] Universidad de Buenos Aires. Facultad de Farmacia y Bioquímica. Departamento de Química Analítica y Fisicoquímica. Cátedra de Química General e Inorgánica.

[2] Universidad de Buenos Aires. CONICET. Instituto de Bioquímica y Medicina Molecular (IBIMOL), Facultad de Farmacia y Bioquímica.

[3] NC State University, Plants for Human Health Institute, Animal Science Department.

[4] Department of Life Sciences and Biotechnology, University of Ferrara, Ferrara, Italy.

[5] Universidad de Buenos Aires. Facultad de Farmacia y Bioquímica. Departamento de Química Analítica y Fisicoquímica. Cátedra de Química Analítica Instrumental.

[6] Universidad de Buenos Aires. CONICET. Instituto de Química y Metabolismo del Fármaco (IQUIMEFA), Facultad de Farmacia y Bioquímica.

[7] Universidad de Buenos Aires. Facultad de Farmacia y Bioquímica. Departamento de Química Analítica y Fisicoquímica. Cátedra de Fisicoquímica.

[8] Universidad de Buenos Aires. Facultad de Farmacia y Bioquímica, Departamento de Fisicomatemática. Cátedra de Física.

[9] Universidad de Buenos Aires, Facultad de Farmacia y Bioquímica, Departamento de Tecnología Farmacéutica. Cátedra de Tecnología Farmacéutica I, Buenos Aires, Argentina.

10 Kyung Hee University, Department of Food and Nutrition, Seoul South Korea

*Giuseppe Valacchi and Pablo Evelson share senior authorship.

Correspondence: Pablo Evelson. Universidad de Buenos Aires. Facultad de Farmacia y Bioquímica. Departamento de Química Analítica y Fisicoquímica. Cátedra de Química General e Inorgánica. Junín 956 (1113) Buenos Aires. Argentina. Phone: 5411-5287-4254.

email: pevelson@ffyb.uba.ar

Graphical abstract

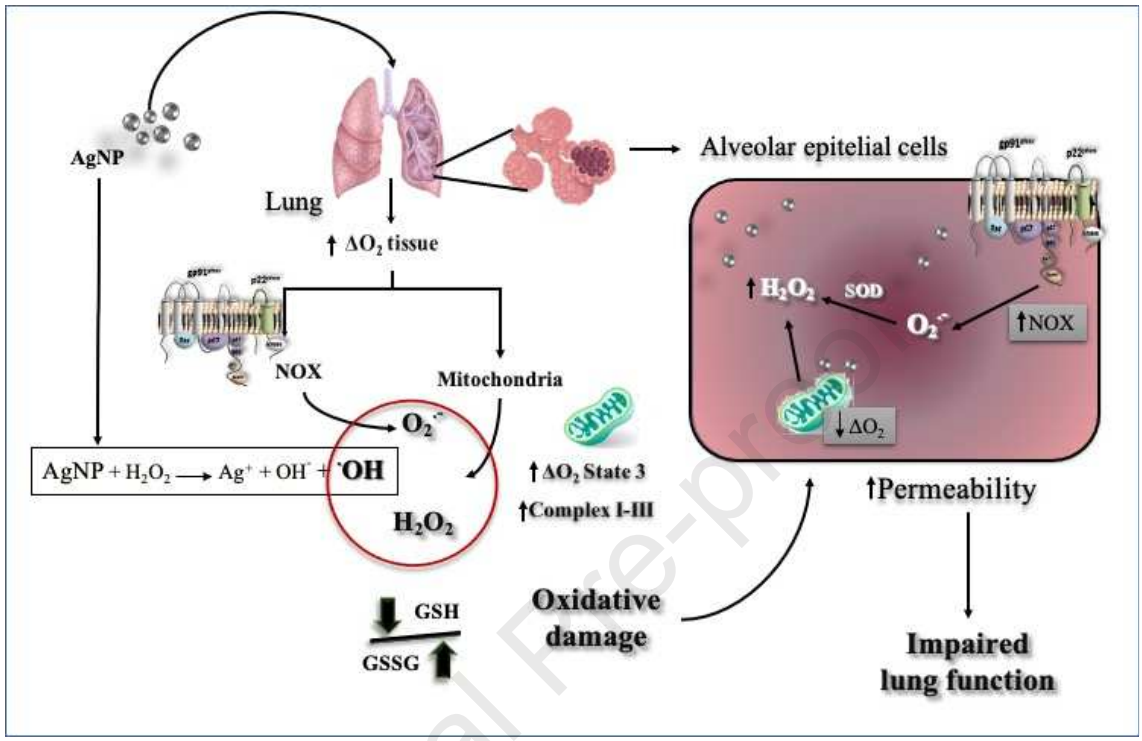

Highlights

- Exposure to AgNP altered lung tissue O_2 consumption due to increased mitochondrial active respiration and NOX activity.
- Increased NOX activity and mitochondrial H_2O_2 production rate led to oxidative damage.
- Lung 3D tissue model showed AgNP-initiated barrier alterations as TEER values decreased.
- Oxidative damage may be responsible for the impaired lung function observed due to alveolar epithelial injury.

Abstract

Along with the AgNP applications development, the concern about their possible toxicity has increasingly gained attention. As the respiratory system is one of the main exposure routes, the aim of this study was to evaluate the harmful effects developed in the lung after an acute AgNP exposure. *In vivo* studies using Balb/c mice intranasally instilled with 0.1 mg AgNP/kg b.w, were performed. ^{99m}Tc-AgNP showed the lung as the main organ of deposition, where, in turn, AgNP may exert barrier injury observed by increased protein content and total cell count in BAL samples. *In vivo* acute exposure showed altered lung tissue O_2 consumption due to increased mitochondrial active respiration and NOX activity. Both O_2 consumption processes release ROS triggering the antioxidant system as observed by the increased SOD, catalase and GPx activities and a decreased GSH/GSSG ratio. In addition, increased protein oxidation was observed after AgNP exposure. In A549 cells, exposure to 2.5 μg/mL AgNP during 1 h resulted in augment NOX activity, decreased mitochondrial ATP associated respiration and higher H_2O_2 production rate. Lung 3D tissue model showed AgNP-initiated barrier alterations as TEER values decreased and morphological alterations. Taken together, these results show that AgNP exposure alters O_2 metabolism leading to alterations in oxygen metabolism lung toxicity. AgNP-triggered oxidative damage may be responsible for the impaired lung function observed due to alveolar epithelial injury.

Keywords: nanoparticles, lung epithelium, nanotoxicology, oxidative metabolism, NADPH oxidase, mitochondria.

List of abbreviations

4-HNE, 4-hydroxynonenal

AgNP, silver nanoparticles

DMPO, 5,5-Dimethyl-1-pyrroline N-oxide

GSH, reduced glutathione

GSSG, oxidized glutathione

HO-1, heme oxygenase 1

NP, nanoparticles

NOX, NADPH oxidase

ROS, reactive O_2 species

SOD, superoxide dismutase

TEER, transepithelial electrical resistance

TBARS, Thiobarbituric acid reactive substances

Introduction

Nanoparticles (NP) have been defined as materials presenting a size range between 1 and 100 nm, in at least one external dimension [1,2]. The reason why the NP use became attractive for a numerous of applications is based on their unique feature of a high surface to mass ratio given by their small size [3]. The nanotechnology field has grown exponentially over the last decades with a production of NP that are mainly used for electronics, cosmetic, food technology, biological sensors, and biomedical purposes. Among the over 1800 products containing nanomaterials currently available, about 25% of them present silver nanomaterials in their composition. Silver nanoparticles (AgNP) are widely used given their activity as antibacterial, antifungals and antivirals [4]. Mechanisms behind AgNP activity against different organisms are adhesion onto the cell wall surface and membrane, penetration into the cell and intracellular structures and biomolecules destabilization. AgNP may induce oxidative stress and signal transduction pathways modulation [~~5~~,~~6~~,5,6]. Those processes depend on several morphological and physicochemical characteristics (e.g., size, shape, surface, and composition) [7,8]. For instance, AgNP effectiveness relies on their size, in fact particles with a size range between 10 and 15 nm exhibit increased stability, biocompatibility and enhanced antimicrobial activity [9,~~12~~,10] and even smaller particles (1 to 10 nm) have been found to display better antimicrobial activity [~~14~~,~~15~~,11]. The small particle size and corresponding large surface/area confer specific properties, which can be either positive and desirable or negative and undesirable, or even a mix of both [12].

The production, use, and disposal of nanomaterials can lead to increased amounts of AgNP release into the air, water, and soil [6,13,~~18~~,14], rising concern about the potential adverse effects on human health upon exposure to AgNP. Human exposure to AgNP may take place through various routes, including the respiratory tract, the skin, the gastrointestinal tract, the reproductive system, or the circulatory system. Moreover, AgNP inhalation is considered one of the most important entry points since the respiratory system serves as a major portal for ambient particulate materials. The widespread use of domestic products containing AgNP such as deodorants, shoe spray or cleaning products could also lead to accidental AgNP inhalation [4,6], which could be even more pronounced in workers handling these NP. Although several occupational guidelines and exposure limits for airborne silver have been proposed, until now, a consensus on occupational exposure limits (OEL) for nanomaterials have not been

reached. The World Health Organization (WHO) has developed guidelines with recommendations on protection from nanomaterials´ potential risks, where AgNP are named as one the most relevant NP being produced requiring an OEL [15]. Therefore, the study of the AgNP inhalation negative impact on human health became one of the most important nanotoxicology concerns.

As the same mechanisms through which AgNP exert their antipathogenic activity could initiate toxic effects, including tissue inflammation and oxidative stress, causing abnormal function or cell death [16,17,19], the aim of the present work was to investigate the mechanisms of the AgNP harmful effects on the cellular redox homeostasis in the respiratory system.

Materials and Methods

Drugs and Chemicals

All chemicals were purchased from Sigma-Aldrich chemical company (St. Louis, MO, US), except for HCl, H_2SO_4, and organic solvents which were purchased from Merck KGaA (Darmstadt, Germany) and antibodies 4-hydroxynonenal (AHP 1251, BIORAD), heme oxygenase 1 (VPA00553, BIORAD) and β-actin (13ES, Cell Signaling Technology).

AgNP characterization

Electron microscopy

AgNP size and morphology were analyzed by Scanning Electron Microscopy (SEM) and Transmission ElectronMicroscope (TEM). A drop of the NP suspension was air dried onto a carbon film-coated grid. Afterwards, SEM was assessed in a Zeiss EVO 40 (Carl-Zeiss, Oberkochen, Germany) at 500000 K.X. In parallel, a drop of the sample in aqueous media was deposited on 400-mesh carbon-coated copper grids, dried and subsequently TEM analysis was performed in a Zeiss EM 109T (Carl-Zeiss, Oberkochen, Germany) at 2500000 X [19].

Hydrodynamic diameter and zeta potential

The hydrodynamic diameter, size distribution and zeta potential of the AgNP were measured by Dynamic Light Scattering (DLS, scattering angle of θ=173° to the incident beam, Zetasizer Nano-ZSP, ZEN5600, Malvern Instruments, United Kingdom) at 25 °C. Samples were equilibrated for 5 min at 25 °C before each measurement. Results were expressed as mean (nm) ± standard deviation (S.D.), n=3 [~~25~~, 20].

Ag^+ desorption assay

Ag^+ release from the AgNP was evaluated by atomic absorption spectrometry. Measurements were performed by collecting samples of AgNP suspension at room temperature for up to 24 h. The AgNP suspension was collected at different time points and filtered using a Vivaspin TM ultrafiltration device (30 kDa MWCO, Sartorius Stedim Biotech Gmbh). The filtered aliquot was analyzed with a VGP 210 atomic absorption spectrophotometer (BuckScientific, East Norwalk, CT, USA) employing electrothermal atomization using pyrolytic graphite tubes [21].

AgNP Fenton-like chemistry

H_2O_2 was generated by the glucose/glucose oxidase system and followed by the Amplex Red-horseradish peroxidase (HRP) method [22]. H_2O_2 consumption by the addition of AgNP was measured as an index of their ability to induce Fenton-like chemical reactions. After an initial stabilization period, 1 mM glucose and 1 ng/mL glucose oxidase were added to the reaction mixture. Resorfurin formation due to Amplex Red (25 μM) oxidation by HRP (0.5 U/mL) bound to H_2O_2 was measured in Perkin Elmer LS 55 Fluorescence Spectrometer (Perkin Elmer, Waltham, MA, US) at 563 nm (excitation) and 587 nm (emission). Subsequently, 2 μg AgNP/mL and 4 μg AgNP/mL were added. A calibration curve was performed using H_2O_2 solutions as standard and H_2O_2 production rate was expressed as pmol/min [23].

Electron paramagnetic resonance (EPR) spectroscopy

EPR was employed to measure the hydroxyl radical ($OH^{\bullet}$) produce from the hemolytic cleavage of H_2O_2. AgNP was mix with the spin trap 5, 5-dimethyl-1-pyrroline N-oxide DMPO (25 mM) and H_2O_2 (200 mM) in a phosphate buffer solution (pH 7.2), and then transfer into a 100 μl quartz capillary tube. After 15 min, the EPR spectrum was recorded using EPR spectrometer (Bruker Analytik GmbH Rheinstetten, Germany). The DMPO-$OH^{\bullet}$ EPR spectrum produced by AgNP was recorded in the presence of desferroxamine (2 mM) in the reaction media to discard ferric anions contamination. Experimental conditions as follows: magnetic field, 336.5 ± 5.0 Mt; power, 1mW; modulation frequency, 9.41 GHz; amplitude, 1 x 200; sweep time, 4 min. The DMPO-$OH^{\bullet}$ adduct is characterized by the four-line spectrum shown of intensity 1:2:2:1 [24].

Animal exposure

Female Balb/c mice weighing 20-25 g were exposed to saline solution (control group) or AgNP suspensions by the nasal drop technique as previously described [25]. Briefly, mice were lightly anaesthetized (i.p.) with ketamine (10 mg/kg body weight) and xylazine (0.1 mg/kg body weight), and intranasally instilled with two bolus of 50 μL of the AgNP suspension (0.1 mg AgNP/kg body weight). Normalizing the surface area of the respiratory zone, the delivered AgNP dose to each mouse in the present work (2.5 μg) would equate to ≈ 5 mg lung burden in humans. Taking into account that 10 nm NP lung deposition is approximately 50% [26], the actual AgNP mass reaching mouse

lungs would be 1.25 µg, which is the same as 2.5 mg in humans. Considering that minute ventilation is 7500 mL/min at rest, the administered dose would be achieved by an exposure to levels under 100 $\mu g/m^3$ in an 8 h/day exposure during a week. Therefore, the AgNP dose administered, was consistent with the Occupational Safety and Health administration (OSHA), the National Institute for Occupational Safety and Health (NIOSH) and the American Conference of Governmental Industrial Hygienists (ACGIH) occupational exposure limit (OEL) proposed of 100 $\mu g/m^3$ for a 40 h work week [4, 27] and also used in previous *in vivo* studies [28,29]. Animals were sacrificed 1 or 24 h after the exposure to saline solution or AgNP by anesthesia overdose. Afterwards, lung samples were collected. All experimental animal protocols were approved by the Animals Ethics Committee of the School of Pharmacy and Biochemistry, University of Buenos Aires (Reference number 2346/18). All procedures were carried out in accordance with institutional guidelines.

Biodistribution studies of radiolabeled AgNP

Briefly, 150 µL of an AgNP suspension (0.02 mg/mL) was incubated with BH_4Na (10 mg) for 2 min at room temperature. Afterwards, 10.7 MBq (0.3 mCi, approximately 300 µL) of $^{99m}TcO_4^-$ eluted from a ^{99}Mo-^{99m}Tc generator (Laboratorios BACON, Argentine) were added to the AgNP suspension and incubated for 10 min. The radiolabeling efficiency of AgNP was tested by thin layer chromatography using instant thin layer chromatography silica gel (ITLC-SG) strips as stationary phase and methylethylketone as the mobile phase. The radiolabeling yield, expressed as a percentage of the total amount of radioactivity applied in the testing system, resulted > 90%. Female Balb-c mice weighing 20-25 g were exposed to ^{99m}Tc-AgNP by the nasal drop technique as previously described in *Animal exposure*. Control mice were handled in parallel and instilled with 50 µL of ^{99m}Tc. After 1 and 24 h, biodistribution static images were obtained at ventral position using a gamma camera equipped with a high-resolution parallel hole collimator, a 256 x 256 matrix, a 1.5 zoom, and collecting more than $1.5x10^6$ counts. After the image acquisition, animals were euthanized, and organs were removed. Activity in each organ was measured using a solid scintillation counter and after correction for efficiency and decay, was expressed as a percentage of total radioactive activity in the tissue (corrected by the total radioactivity in the mouse) per gram of tissue (total activity/ g tissue).

A549 immortalized cells line and EpiAirway™ primary cultures exposure

A549 cells were cultured in Dulbecco's modified Eagle's medium high glucose (DMEM) supplemented with 10% fetal bovine serum (FBS), 2 mM glutamine, penicillin, and streptomycin 1%. Cells were maintained in a humidified atmosphere with 5% CO_2 at 37°C and media refreshed every 2-3 days until the ideal confluence was reached as previously described [30].

AgNP suspension was freshly prepared by resuspending then in culture media (DMEM) at final concentration of 2.5 µg/mL, followed by 10 min incubation in an ultrasonic water bath. DMEM without AgNP was used as a control group. After reaching 80–90% confluence, the cells were exposed to 0.5, 1.0, 2.5 and 5 µg/mL of AgNP suspensions for 1 h, using DMEM without AgNP as control group. After exposure, fresh culture medium was added to each well and then samples were collected at 1, 3 and 24 h for the different assays.

EpiAirway, a 3D cell culture model of primary human tracheal and bronchial epithelial cells from MatTek, was used as a model of lung (AIR-100-SNP, MatTek Corporation, Ashland, MA). As described above, AgNP suspensions were freshly prepared at 2.5 µg/mL in tissue culture medium and topically applied on the apical surface of EpiAirway tissues for 1 h, using PBS as control group. Fresh tissue culture medium was added in the basolateral surface of each insert. After 1 h of exposure, EpiAirway tissues were gently rinsed with DPBS (Dulbecco's phosphate buffered saline) to remove AgNP suspensions and PBS (control group) from the apical surface. Then, tissue inserts were transferred to wells containing fresh medium. EpiAirway tissues, basolateral supernatants and apical washes were collected at 24 h post-exposure.

Cytotoxicity determination in A549 cells and EpiAirway 3D tissues

Twenty-four hours after AgNP exposure, A549 cell culture media, EpiAirway tissue culture media and apical washes were collected. Cytotoxicity was determined by lactate dehydrogenase (LDH) release in the media, measured by enzymatic assay: in the first step NAD^+ is reduced to $NADH/H^+$ by the LDH-catalyzed conversion of lactate to pyruvate; in the second step the catalyst (diaphorase) transfer H/H+ from $NADH/H^+$ to tetrazolium salt which is reduced to formazan. The amount of LDH in the supernatants was determined and calculated according to kit supplier´s instructions. All tests were performed in triplicate. Results are expressed as the percentage of change relative to control values.

Samples preparation

Tissue cubes

After the exposure to AgNP, animals were sacrificed and lung samples were removed and immediately placed in ice-cold Krebs buffer solution [118 mM NaCl, 4.7 mM KCl, 1.2 mM KH_2PO_4, 1.2 mM $MgSO_4$, 2.5 mM $CaCl_2$, 24.8 mM $NaHCO_3$, and 5.5 mM glucose (pH 7.4)]. After being washed and weighted, 1 mm^3 tissue cubes were cut by the use of a scalpel [31].

Tissue homogenates

Lung samples (0.2 g of wet weight) were homogenized (1:5) with a glass-Teflon homogenizer in a medium consisting of 120 mM KCl, 30 mM phosphate buffer (pH 7.4) at 4 ºC. The suspension was centrifuged at 600 *g* for 10 min at 4 ºC to remove nuclei and cell debris. The pellet was discarded, and the supernatant was used as "homogenate" [32].

Mitochondria isolation and, preparation of mitochondrial membranes

Lung mitochondria purified fractions were obtained from lung homogenates by differential centrifugation in a Sorvall RC5C centrifuge (Sorvall, Buckinghamshire, England). Briefly, lungs were washed, and mixed in ice-cold STE buffer [250 mM sucrose, 5 mM Tris–HCl, and 2 mM EGTA (pH 7.4)]. Samples were centrifuged at 700 g for 10 min to discard nuclei and cell debris. The sediment was discarded, and the supernatant was centrifuged at 8000 g for 10 min to obtain the enriched mitochondria fraction. The mitochondrial pellet was washed twice and resuspended in a minimum volume of the same buffer. The whole procedure was carried out at 0–4 °C. Purity of isolated mitochondria was assessed by determining lactate dehydrogenase activity; only mitochondria with less than 3% of cytosolic lactate dehydrogenase activity were used [33].

Mitochondrial membranes were obtained by three freeze-thaw cycles of the mitochondrial preparation, followed by the homogenization step by passage through a 29G hypodermic needle [34].

Bronchoalveolar lavage (BAL)

BAL samples were taken using a 226 x 1" catheter into the mouse trachea. After removing the stylet hub, the catheter and the trachea were tied together firmly with a nylon string. Using a 1 mL syringe, 0.8 mL of PBS was loaded 4 times. Finally, the catheter was removed from the syringe and the recovered lavage fluid was saved in 1.5 mL Eppendorf tubes on ice.

Cell lysate

A549 cells were washed with ice-cold PBS and lysed in ice-cold lysis Buffer (20 mM TRIS pH 8, 150 mM NaCl, 1% Triton X-100, 1 mM sodium orthovanadate, 1 µg/mL aprotinin 1 µg/mL pepstatin, 1 µg/mL PMSF, and 5 mM β-glycerophosphate). The suspensions were centrifuged at 14000 g for 15 min at 4°C, the pellet was discarded, and the supernatants were collected.

Oxygen consumption

Oxygen consumption by lung tissue cubes

A two-channel respirometer for high-resolution respirometry (Hansatech Oxygraph, Hansatech Instruments Ltd, Norfolk, England) was used. O_2 consumption rates were measured at 30 °C in Krebs buffer solution ~~[41]~~. KCN (4 mM) was added to the reaction chamber as a mitochondrial cytochrome oxidase inhibitor [31]. Results were expressed as ng-at O/min g tissue.

Mitochondrial oxygen consumption

Lung mitochondrial O_2 consumption was followed polarographically with a clark-type O_2 electrode (Hansatech Oxygraph, Hansatech Instruments Ltd, Norfolk, England) for high resolution respirometry at 30°C. Freshly isolated lung mitochondria (0.15 mg proteins/mL) were incubated in a respiration buffer (120 mM KCl, 5 mM KH2PO4, 1mM EGTA, 3 mM HEPES, and 1 mg/mL fatty acid-free BSA, pH 7.4) supplemented with 2 mM malate and 5 mM glutamate. An initial rest state respiration (state 4) was established under these conditions, which was then switched to active state respiration (state 3) by the addition of 125 µL ADP. Respiratory control ratio (RCR) was calculated as state 3/ state 4 respiration rates [33]. Results were expressed as mg-at O/min. mg proteins.

Cellular oxygen consumption rate (OCR) assays in A549 cell line

The XF-24 Extracellular Flux Analyzer (Seahorse Biosciences, Billerica, MA) was used to measure the oxygen consumption rate (OCR). A549 cells were seeded at density 30000 per well and allowed to grow overnight. The cells were then exposed to AgNP for 1 h a dose of 2.5 µg/mL.

Plates were kept at 37°C in a non-CO2 incubator for 60 min and loaded into the Seahorse XF-24 extracellular flux analyzer following the manufacturer's instructions. All experiments were performed at 37°C. Baseline measurements of OCR and ECAR were performed at beginning of the assay, and these were followed by the sequential addition of ATP synthase inhibitor (oligomycin), an uncoupler of oxidative phosphorylation (FCCP) and an inhibitory of complex III (antimycin). Generally, four baseline measurements and three response rates were measured, and the average of these rates used for data analysis.

Cells were first titrated with 1-4 µM of FCCP. Two µM FCCP gave the maximum oxygen consumption rate, so that concentration was used for the experiments. Non-mitochondrial oxygen consumption rate was determined after the addition of 5 µM antimycin and subtracted from all other values before calculation of the respiratory parameters as previously described [35]. Respiratory parameters are obtained as follows: basal respiration, baseline; respiration driving ATP synthesis, basal respiration-respiration proton leak; maximum respiration control ratio (RCR), maximum respiration/respiration driven proton leak [~~43,~~36]. The results were expressed as pmol/min.

NADPH oxidase (NOX) activity

NOX activity in lung homogenates

The lucigenin-derived chemiluminescence method was used as an indirect measurement of NOX activity [37]. Briefly, 50 µg of protein tissue homogenate was diluted in 250 µL of 50 mM phosphate buffer containing 1 mM EGTA and 150 mM sucrose (pH 7.4). Lucigenin (50 µM) was added to the reaction media, 100 µM NADPH was used as substrate, and chemiluminescence was immediately measured at 15 s intervals for 3 min in a microplate reader (Varioskan LUX, Thermo Scientific, Massachusetts, USA) In addition, assay specificity was confirmed using superoxide dismutase (SOD) (200 U/mL). Results were expressed in arbitrary units (AU)/mg protein.

NOX activity in A549 cells

The lucigenin-derived chemiluminescence method was used as an indirect measurement of NOX activity in the membrane fraction obtained from A549 cells. After 1 and 3 h cells were washed twice with PBS and scraped in a buffer (10 mM Tris-HCl pH 7.5, 1 mM EDTA, 1 mM EGTA). Cells were separated from the buffer by centrifugation at 500 g during 5 min. Next, cells were resuspended in 250 µL of 50 mM phosphate buffer containing 1 mM EGTA and 150 mM sucrose (pH 7.4). Lucigenin (50 µM) was added to the reaction media, 100 µM NADPH was used as substrate, and chemiluminescence was continuously measured for 3 min in a Varioskan LUX microplate reader (Thermo Fisher Scientific). The specificity of the assay was confirmed by the addition of SOD (200 U/ml) as an O_2•− scavenger. Results were expressed in arbitrary units (AU)/mg protein [33, 38].

Mitochondrial complex activity.

Mitochondrial NADH-cytochrome c reductase (Complexes I-III) activity

Complexes I-III activity was evaluated by a colorimetric assay following cytochrome c3+ reduction rate at 550 nm (ε = 19 mM^{-1} cm^{-1}) and 30°C [33]. Mitochondrial membranes (1.0 mg prot./mL) were added to 100 mM phosphate buffer (pH 7.2), supplemented with 0.2 mM NADH, 25 µM cytochrome c3+ and 0.5 mM KCN and measured in a microplate reader (Varioskan LUX, Thermo Scientific, Massachusetts, USA. Results were expressed as nmol reduced cytochrome c3+/min mg prot.

Succinate cytochrome c reductase (Complexes II-III) activity

Complexes II-III was determined by a colorimetric assay following cytochrome c3+ reduction rate at 550 nm (ε = 19 mM^{-1} cm^{-1}) and 30°C [34]. Mitochondrial membranes (1.0 mg prot./mL) were added to 100 mM phosphate buffer (pH 7.2), supplemented with 0.5 mM succinate, 25 µM cytochrome c3+ and, 0.5 mM KCN and measured in a microplate reader (Varioskan LUX, Thermo Scientific, Massachusetts, USA. Results were expressed as nmol reduced cytochrome c3+/min mg prot.

Cytochrome oxidase (Complex IV) activity

Complex IV was assayed spectrophotometrically at 550 nm by following the oxidation rate of 50 mM cytochrome c^{2+} in 0.1 M K_2HPO_4/KH_2PO_4 (pH 7.4), 50 µM cytochrome c^{2+}, and 0.02 mg/mL mitochondrial membranes [34]. Results were expressed as k'/mg prot.

H_2O_2 production rate

Mitochondrial H_2O_2 production rate.

Mitochondrial H_2O_2 production rate was evaluated by the Amplex Red-HRP method as described in Materials and Methods (NP Fenton-like Chemistry). Malate (2 mM) and glutamate (5 mM) were used as mitochondrial respiratory substrates. After an initial stabilization period, freshly isolated lung mitochondria (0.25 mg protein/mL) were added to the reaction mixture. Controls in the absence of isolated mitochondria or HRP indicate that nonspecific probe oxidation was kept at minimum (<1%). Results were expressed as nmol/min mg protein [39].

H_2O_2 production rate in A549 cells

To study ROS generation from freshly suspended A549 cells exposed to AgNP, H_2O_2 production was measured by fluorescence spectroscopy using the Amplex Red/horseradish peroxidase (HRP) system. At 1 and 3 h after AgNP exposure, A549 cells were detached from the plates and incubated in a reaction medium (125 mM sucrose, 65 mM KCl, 10 mM HEPES, 2 mM KH_2PO_4, 2 mM $MgCl_2$, 0.01% BSA, pH 7.2) in the presence of 25 μM Amplex Red, 0.5 U mL-1 HRP, and 2 mM malate and 5 mM glutamate as substrates. Resorufin fluorescence intensity (the product of Amplex Red oxidation by H2O2/HRP) was measured in a microplate reader (Biotek microplate reader, Winnoski, VT, USA) at λex = 563 nm; λem = 587 nm. A calibration curve was obtained using H_2O_2 as standard. Results were expressed as nmol H_2O_2 min^{-1} mg $prot^{-1}$ [22].

Antioxidant system

Antioxidant enzymes activity

Superoxide dismutase (SOD) activity was determined spectrophotometrically by following the inhibition of the rate of adenochrome formation at 480 nm, in a reaction medium containing 1 mM epinephrine and 50 mM glycine/NaOH (pH 10.5) [~~48~~,40]. Enzymatic activity was expressed as SOD units/mg proteins. One SOD unit was defined as the amount of sample able to inhibit the rate of adenochrome formation by 50%. Catalase activity was evaluated by following the decrease in absorbance at 240 nm in a reaction medium consisting of 100 mM phosphate buffer (pH 7.4) and 20 mM hydrogen peroxide [40,41]. Results were expressed as pmol catalase/mg protein.

Glutathione peroxidase (GPx) activity was determined in lung tissue homogenates in the presence of glutathione reductase enzyme, following the oxidation of NADPH at 340 nm [40]. Results were expressed as nmol/ min.mg protein.

Reduced glutathione (GSH) and oxidized glutathione (GSSG) levels

Lung and heart samples were homogenized with a glass-Teflon homogenizer in a relation 1/7 with MSTE and centrifuged at 800 g for 10 min at 4°C. After centrifugation, 30 µL of supernatant was mixed with 60 µL of trifluoroacetic acid 10%-EDTA 1mM. Afterwards, samples were centrifuged at 20000 *g* for 20 min at 4 °C. Supernatants were filtered through 0.22 µm cellulose acetate membranes (Corning Inc., NY, US), and frozen at -80 °C until use. HPLC analysis was performed in a HPLC Ultimate 300 (Thermo Scientific, CA, USA) using a microcolumn BSD Hypersil C18, Thermo Scientific (100x2.1 mm d.i and 2.4 µm) and a mass detector TSQ Quantum Acess Max (Thermo Fisher Scientific, CA, USA). GSH and GSSG were eluted at a flow rate of 0.2 mL/min with methanol:ammonium formiate (1:99) (pH 3.5). Results were expressed as mg/g tissue [40,51].

Protein oxidation

Carbonyl groups content from oxidized proteins were determined in lung tissue homogenates spectrophotometrically with 10 mM 2,4-dinitrophenylhydrazine (DNPH). The formation of a stable 2,4-dinitrophenylhydrazone product (DNP) soluble in 6 M guanidine was measured at 370 nm [42]. Results were expressed as nmol/mg protein.

Histology

EpiAirway tissue was fixed in 10 % buffered formaldehyde and embedded in paraffin. For histological observation, the sections (4µm thickness) were deparaffinized in xylene and rehydrated in alcohol gradients and then stained with hematoxylin and eosin [43].

Total cell number in BAL

Centrifuge BAL at 800 g for 10 min at 4°C for obtained cells and were counted in a Neubauer chamber.

Transepithelial electrical resistance (TEER) of EpiAirway 3D tissue

Airway barrier integrity was determined by measuring transepithelial electrical resistance (TEER) with an EVOM2 voltohmmeter and a 12 mm EndOhm electrode chamber. Before measurement, electrodes were equilibrated and sterilized according to the manufacturer's recommendations. After 24 h of the initial exposure the apical surface of the EpiAirway was rinsed 3 times with PBS. Two hundred microliters of PBS were added in the upper compartment of the cell culture system. The ohmic resistance of a blank (culture insert without cells) was measured in parallel. To obtain the sample resistance, the blank value was subtracted from the total resistance of the sample. The final unit area resistance (Ω*cm^2) was calculated by multiplying the sample resistance by the effective area of the membrane (0.6 cm^2) [44].

Western blot analysis in A549 cells

At each experimental time point, equal amounts of the cell lysate protein extracts were resolved by 10% sodium dodecyl sulfate-polyacrylamide gel electrophoresis and, then, electro-blotted onto nitrocellulose membranes by use of Trans-Blot Turbo transfer system (Bio-Rad). Blots were blocked in Tris-buffered saline, pH 7.5, containing 0.5 % Tween 20 and 5% milk for 1h. Membranes were incubated overnight at 4°C with the appropriate antibodies: 4-hydroxynonenal (4-HNE) (AHP1251, BIORAD), Heme oxygenase 1 (HO-1) (VPA00553 BIORAD) and, β-actin (13ES, Cell Signaling Technology). Membranes were then incubated with horseradish peroxidase-conjugated secondary antibody for 1h. Immunoblots were developed with a chemiluminescence detection kit (ECL from BIORAD), using β-actin as loading control. Images were taken using a ChemiDoc MP Imaging System (BIORAD). Densitometry analysis of the bands was performed using ImageJ (National Institutes of Health, Bethesda, MD, USA). Protein band densities were normalized to the β-actin expression.

Protein content

Protein concentration of tissue homogenates and BAL samples was measured by the method of Lowry et al [45] using BSA as standard. Protein concentration of A549 cell line samples was measured by the method of Bradford et al [46], using BSA as standard.

Results

AgNP characterization

AgNP were characterized in terms of morphology, diameter, aggregation tendency and size distribution. First, morphology was assessed by TEM and SEM and, as shown in Figure 1A and 1B, respectively, AgNP were mainly spherical shaped with a diameter of 9.0 ± 1.2 nm. The DLS analysis showed a hydrodynamic diameter of 16.8 ± 5.9 nm where only one size population was observed. Moreover, the colloidal dispersion exhibited a narrow size distribution according with the polydispersity index (PDI) of the sample (0.196 ± 0.043). This index is dimensionless, values less than 0.300 are acceptable and indicate a homogenous population [47]. According to these results, AgNP were stable as no agglomeration was evidenced. The DLS also showed a negative zeta potential value of -40 mV. A colloidal dispersion is considered stable if the zeta potential value is below -30 mV or above +30 mV. Desorption studies, when AgNP suspension was kept at room temperature, showed a 24% Ag^+ release after 1 h a maximum of 34 % after 4 h when reached a plateau for up to 24 h (Figure 1C). Transition metals such as Ag can participate in Fenton-like chemical reactions, in which the hemolytic H_2O_2 cleavage generates $OH^{\bullet}$. As it shown in Figure 1D, the AgNP suspension significantly consumed the H_2O_2 levels produced by the glucose/glucose oxidase system in a concentration-dependent manner (basal: 42.0 ± 1.3 pmol/min, AgNP100: 33.0 ± 1.5 pmol/min, AgNP200: 26.0 ± 2.3 pmol/min). A solution prepared with an equivalent amount of Ag as the one present in 200 µL of AgNP suspension Ag (I) did not change H_2O_2 levels produced when compared to basal. These results showed that AgNP were able to consume H_2O_2 by a Fenton-like reaction, suggesting that it might be a relevant mechanism of $OH^{\bullet}$ production. To further confirm the generation of $OH^{\bullet}$ produced from the hemolytic cleavage of H_2O_2, we used EPR spectroscopy using DMPO as a probe in order to form the DMPO-$OH^{\bullet}$ adduct. Our findings indicate that in AgNP samples incubated with DMPO we were able to detect the four-line characteristic DMPO-$OH^{\bullet}$ adduct spectrum, which represents the presence of the $OH^{\bullet}$ (Figure 1E).

Lung is the main AgNP deposition organ after inhalation

There is evidence that NP or NM reaching the lower respiratory airways can translocate into systemic circulation [48,49]. Hence, the AgNP ability to deeply penetrate into the lung, break through the respiratory epithelia and reach the secondary organs was evaluated through biodistribution studies after ^{99m}Tc-radiolabeled AgNP intranasal instillation in Balb/c mice. The representative whole body AgNP biodistribution image showed that the lung is the organ with the higher AgNP deposition, both at 1 and 24 h after treatment (Figure 2A and 2C). In agreement with the signal obtained by the gamma camera, the *ex vivo* distribution studies showed the lungs as the site with higher NP accumulation, as evidenced by the 73% of total radioactivity/ g tissue followed by the stomach (23%) and the administration point (3%) (Figure 2B). Moreover, NP remained lodged in the lungs (93% total activity) 24 h after radiolabeled AgNP inhalation while only 4% was found in the stomach (Figure 2D). The signal obtained in other organs, at both time points analyzed, was less than 1% or not detectable (data not shown). Biodistribution results showed that there is no evidence of AgNP translocation at the time period studied in our model; the AgNP reached the lung and remained there up to 24 h after inhalation. With the aim of further evaluating the consequences of the AgNP over the lung epithelial barriers functionality, studies in BAL of mice exposed to AgNP suspension for 24 h were performed. The BAL protein levels showed a 46% increase in the AgNP compared to control values (control: 0.50 ± 0.05 mg/mL, $p<0.05$) (Figure 2E). Moreover, as shown in Figure 5F, the BAL total cells count was 2 times higher in animals treated with AgNP than in control mice (control: $45x10^4 \pm 15x10^4$ cells, $p<0.05$). Our results suggest that the presence of AgNP in lung tissue compromised the integrity of the epithelial barriers.

Inhalation of AgNP produced an alteration in the lung O_2 metabolism

We analyzed lung tissue O_2 consumption from mice exposed to saline (control) or AgNP suspension as a first approach to assess O_2 metabolism. Figure 3A shows a representative trace of O_2 consumption after exposure to AgNP or saline. Tissue O_2 consumption was significantly increased by 31% after AgNP exposure when compared with the control group (control: 310 ± 23 ng-at O/min g tissue, $p<0.05$) (Figure 3B). As we and others have previously shown, mitochondrial respiration and oxidase and oxygenase enzymes, such as NOX, might also play a relevant role as ROS production

sources after NP exposure [50], meaning that both mitochondrial respiration and NOX activation could be significant contributors to the observed increase in lung O_2 consumption following Ag-NP exposure.

Consistently, NADPH-dependent superoxide production by lung homogenate increased by 44% in treated animals (control: 43 ± 4 AU/min mg prot., $p<0.05$) (Figure 3C). Moreover, the analysis of the O_2 consumed by isolated mitochondria is the classical approach to characterize mitochondrial function. Table 1 shows mitochondrial rest state (State 4) and active state yielding ATP (State 3) O_2 consumption rates. Mitochondrial metabolic state 3 was significantly increased by 57% in AgNP group when compared to control values (control: 28.0 ± 1.5 ng-at O/min g prot., $p<0.05$). The observed alteration in the organelle function after the exposure of AgNP was further investigated by assessment of mitochondrial respiratory chain complexes activities. Complex I activity was found to be significantly increased by 28% (control: 154 ± 5 nmol/min mg prot., $p<0.01$), whereas no differences were observed in either complex III or IV activity after AgNP inhalation when compared with the control group (Table 2). As shown in Figure 3D, 1 h after the instillation, mitochondrial H_2O_2 production rate was 39% higher in the AgNP group than control animals (control: 1.1 ± 0.1 nmol/min mg prot., $p<0.05$). These observations confirmed that AgNP intranasal instillation hampers proper O_2 handling in the lung, indicating that mitochondrial respiration and NOX activation are both significant O_2 uptake and ROS production sources. The occurrence of lung oxidative damage to proteins was evaluated through the carbonyl content assay. A 46% increase in carbonyl content was observed in the AgNP group compared to the control (control: 12 ± 1 nmol/mg protein, $p<0.05$) (Fig. 3E). Subsequently, we evaluated the low molecular weight antioxidant status through the measurements of GSH and GSSG levels. A 29% decrease in GSH levels was observed in lung homogenates of AgNP group compared to control group (control: 21.5 ± 2.0 µg/mg tissue; *$p<0.05$*), which led to a decreased lung GSH/GSSG ratio (*$p<0.05$*) in AgNP -exposed mice (Figure 3F). Antioxidant enzymes activities in lung homogenates after AgNP exposure were assessed, showing a significant 68% increase in SOD (control: 9.6 ± 1.4 USOD/mg prot., $p<0.05$), along with a 18% increase in catalase and 16% increment in GPx activities when compared to control values (control: 0.8 ± 0.1 pmol/mg prot., $p<0.05$ and control: 88 ± 4 nmol/mg prot., $p<0.05$ respectively) (Figure 3G, 3H and 3I). This scenario suggests an increased exposure to ROS in the lung as a result of impaired O_2

metabolism, which might overwhelm antioxidant defenses and produces oxidative damage to proteins.

AgNP-induced ROS led to lung epithelial cells oxidative damage

To deeply analyze AgNP toxicological mechanisms in lung epithelium, we conducted *in vitro* experiments. First, cytotoxicity was evaluated by LDH release in the media of A549 cells exposed to AgNP for 24 h (Supplementary Figure 1). From the wide AgNP dose rage evaluated, we have chosen 2.5 µg/ml AgNP for further experiments as it did not show LDH release increments. Similar to lung tissue, we evaluated ROS sources after AgNP treatment. We found an increased NOX activity up to 49% after 3 h of exposure to AgNP suspension compared to the control group (control: 13.0 ± 0.8 AU/min mg protein, $p<0.05$) (Figure 4A). In figure 4B, A549 cells showed an increase of 73% in the mitochondrial H_2O_2 production rate after 1 h of exposure to AgNP compared to the control group (control: 4.8 ± 0.6 pmol/s mg prot., $p<0.0001$). An early increase in ROS production may later lead to oxidative damage to macromolecules and expression of antioxidant enzymes. We observed a 23% increase in 4-HNE protein adducts levels (control: 1.1 ± 0.1, $p<0.01$) and a 47% increase in HO-1 expression 24 h after AgNP exposure (control: 0.75 ± 0.06, $p<0.01$) (Figure 4C and 4D). Regarding mitochondrial O_2 consumption source, Figure 5A shows a representative trace of A549 cells O_2 consumption rate (OCR) after exposure to AgNP. Basal OCR (Figure 5B) significantly decreased by 40% in cells treated with AgNP after 3 h (control: 207 ± 15 pmol/min, $p<0.01$). The addition of FCCP allows the determination of the maximal respiration as it uncouples the O_2 consumption from the ATP synthesis. The treatment of A549 cells with AgNP during 3h decreased maximal respiration by 44% compared to the control group (control: 372 ± 32 pmol/min, $p<0.01$), suggesting that lung epithelial cell mitochondria could not respond to an increased energy demand (Figure 4C). Moreover, respiration driving ATP synthesis was also decreased by 32 % after 3 h of AgNP incubation compared to control cells (Figure 4D).

All together, these results suggest an increased ROS production in lung epithelial cells exposed to AgNP as a result of impaired mitochondrial function along with increased NOX activity, leading to oxidative damage.

Exposure to AgNP leads to membrane integrity alteration in a 3D lung tissue model

Exposure to AgNP in EpiAirway tissue, a 3D model consisting of normal, human-derived tracheal/bronchial epithelial cells that recapitulates the *in vivo* respiratory tissue morphology as well as its phenotypical functions such as that of barrier function and mucociliary responses, did not show any cytotoxicity as no difference in LDH release at 24 h post-exposure to 2.5 μg/ml AgNP was found neither in the apical or basolateral supernatants (Figure 6A). Nevertheless, when the lung barrier integrity was assessed by transepithelial electrical resistance (TEER) measurements, an alteration associated with AgNP exposure was found. In fact, as shown in Figure 6B, EpiAirway tissues apically exposed to AgNP for 1h showed a 20% decrease in TEER values after 24 h compared to the control group (control: 871 ± 28 Ω/cm^2, $p<0.01$), suggesting a compromised cellular barrier integrity. Moreover, the tissue morphology evaluation by hematoxilin-eosin staining showed alterations after exposure to AgNP. The 3D stratified tissue model consists 3-4 cell layers including a mitotically active layer of basal epithelial cells and an upper layer of mucus-producing goblet cells. There are also functional tight junctions and beating cilia. As shown in Fig. 6, panel C, PBS-treated control tissue maintains a histologically normal structure and cell organization with a well-preserved stratification of intact airway epithelial cells. Conversely, after topical exposure to AgNP suspension (2.5 μg/mL for 1 hour) (Fig. 6, panel C), 3D tissue model shows a significant damage particularly evident in the apical layer where the cellular architecture appears separated and disorganized compared to the EpiAirway tissues pretreated only with PBS. The upper cells appear compromised with the loss of several cells, which suggests the altered functional cilia and cell junctions with plausible loss of barrier function.

Discussion

Over the last decade, AgNP have become an important nanomaterial utilized in the development of new technologies. However, our knowledge about its associated risk is not yet fully understood [6,51]. Therefore, it seems relevant to establish the toxicological mechanisms triggered by AgNP inhalation, since it would provide valuable information about the possible hazards and risks elicited not only by personal care use of nanomaterials but occupational exposure as well [6]. In the present work, we have studied the effect of a low dose AgNP exposure through *in vivo* and *in vitro* respiratory tissue models.

Compared with microparticles or their bulk of origin, NP possess unique physicochemical properties that correlate with their potential to generate ROS. In this sense, the NP physicochemical characterization, including particle size, surface charge, solubility, and aggregation status release, is a key indicator for the resulting redox response and NP-induced injury since many of these NP intrinsic properties can catalyze the ROS production [52,53]. Accordingly, our physicochemical characterization showed that AgNP were redox active as their reaction involves elemental Ag and H_2O_2 to yield $OH^{\bullet}$ and an oxidized metal ion, effect that was absent when a Ag(I) solution of a similar concentration was tested. This mechanism should be considered as a relevant pathway for AgNP-induced oxidative stress, together with the oxidant generation upon NP interaction with cellular material [52,53,54]. Moreover, possible AgNP surface oxidation could contribute to the release of Ag ions that could amplify the toxicity. Released Ag (I) is suggested to interact with respiratory chain proteins on the membrane, interrupt intracellular O_2 reduction, and induce ROS production, thus exacerbating the oxidative damage produced by AgNP *per se* [~~63~~,55,56]. Therefore, in combination, elemental Ag in the NP and Ag^+ released from the NP core when exposed to biological structures, may exhibit distinctive effects upon toxicological mechanisms in cells that cannot be attributed neither to silver ions alone nor to AgNP exclusively.

In order to achieve meaningful data depicting the possible toxic mechanism after exposure to AgNP levels attained in occupational settings, but by nanosized aerosols release of near the human breathing zone as well [57,58], the AgNP exposure dose selected was consistent with the diverse OEL proposed from important occupational administrations such as OSHA, NIOSH and ACGIH [27,59] and several institutes from

a wide range of countries, with values from 0.098 μg/m^3 up to 50 μg/m^3 [60]. Furthermore, a similar AgNP dose range was used in toxicological studies in experimental animal and cellular systems [28,2970,61].

After inhalation, relatively large particles, or agglomerates (diameter > 1 μm) are likely trapped in the mucus of the upper airways and removed by the mucociliary escalator. However, NP with a diameter < 20 nm are likely to escape the mucus trapping and enter in the deepest zone of the lung [49]. Animal and human studies show that inhaled nano sized particles are removed less efficiently than larger particles by the macrophage clearance mechanisms, being retained in the lung and produce damage, [62] or translocating into the circulatory, lymphatic, and nervous systems to many distant tissues and organs [48,49].

Despite the AgNP size, no evidence for translocated AgNP from lung tissue to extra pulmonary organs was observed at the time points evaluated in this study. Thereby AgNP may compromise the integrity and stability of the cellular junction network, leading to impaired alveolar epithelial function [63]. In fact, here we showed that the AgNP retained in the alveolar region damage the epithelium, making evident the loss of alveolar-capillary barrier integrity, resulting in increased permeability, as evidenced by the higher cell counts in the BAL fluid, which may end up in altered lung function. In this scenario, the analysis of lung O_2 metabolism under AgNP exposure appears to be an important area of study with the aim of understanding reactive O_2 species production mechanisms, which may lead to the onset of respiratory diseases aggravation. Therefore, as a first approach, we studied the effects of AgNP exposure in an *in vivo* model and, afterwards, we further analyzed the mechanism underlying the observed effects through different *in vitro* models.

In the present study, we show that AgNP exposure induces changes in the oxidative metabolism in the lung, through mitochondrial function alteration and the initiation of an inflammatory response, as indicated by increased NOX activity at early time points. As we mentioned before, ROS can be produced by either endogenous or exogenous sources. The endogenous sources of ROS include different cellular organelles such as mitochondria, or enzymatic activity of xanthine oxidase, lipoxygenase, cyclooxygenase, and NOX. We and others have previously shown that the observed oxidative metabolism imbalance following NP exposure within the lung positively correlates with mitochondrial dysfunction and the activation of NOX (a relevant non-mitochondrial source of ROS) [64]. The mechanism of NOX activation has not been completely

elucidated, but previous works have shown that might be connected to the uptake of AgNP by endocytosis/phagocytosis [65]. It is well established that mitochondria also represent an important modulator of cellular responses to a wide variety of metabolic and environmental stressors. Moreover, $O_2^{\bullet-}$ is also produced by the mitochondria under physiological conditions as a byproduct of redox reactions during electron transport in the respiratory chain [66]. In addition to serving as an oxidant production source, mitochondria are highly susceptible to ROS, which could also indirectly perturb the organelle function [33,67,68], leading to organ failure. This might be the case following AgNP exposure, since increased mitochondrial H_2O_2 production was observed in the lung. Consistently, the imbalance toward a pro-oxidant condition following AgNP pulmonary exposure was also associated with a decreased lung antioxidant status (i.e. reduced GSH/GSSG ratio), an increase in protein oxidation and a probable compensatory increase in the activity of antioxidant enzymes such as SOD, catalase and GPx. Previous reports have studied the role of Nrf2 in the antioxidant response [69,70]. In a similar experimental model as the one presented here, Sthijns and colleagues [71] have shown an early adaptive response to AgNP related to an enhanced HO-1 and Nrf2 mRNA expression in A549 human epithelial cells which could explain the increase observed in SOD, catalase and GPx activities in our work. Moreover, autophagy was reported and associated with oxidative stress and increased HO-1 and Nrf2 expression [72].

In addition to our results, a proposed pathway in AgNP adverse effects, upon interaction with biological systems, is the ROS induction. The pro-oxidant environment might be able to interfere with mitochondrial functions, leading to further overproduction of ROS due to mitochondrial damage, which could result in a modulation of the intracellular signaling pathways towards apoptosis, as observed in different studies [56,73]. Moreover, increased ROS production can also overwhelm cellular antioxidant defense capacity, as shown here by the GSH depletion and the increase in protein carbonyl levels in lung tissue. It has already been suggested that changes in the activity of antioxidant enzymes and intracellular GSH levels occur under the influence of AgNP [74].

Alveolar epithelial cells (AEC) are susceptible to the redox imbalance induced by pathogens, inflammatory mediators, hypoxia, hyperoxia, cigarette smoke, air pollutants or even NP exposure. In particular, tight junction proteins in lung epithelial cells are well known targets of oxidative stress damage [75,76~~8076~~] that, leading to alterations in

the transepithelial transport process, compromises epithelial barrier homeostasis and integrity, essential for the tissue physiological activities. Therefore, we conducted *in vitro* experiments in an alveolar epithelial cell line model (A549 cells) exposed to AgNP, in order to establish a mechanism which explains the observations in the whole lung. The *in vitro* AgNP dose was selected based on relevant previous studies [~~82~~77,78,~~85~~].

The loss of redox homeostasis observed as early as 1 h after AgNP exposure was associated with subsequent oxidative damage, indicated by the increased levels in 4-HNE protein adducts and an enhanced expression of the antioxidant enzyme HO-1. Furthermore, in agreement with whole lung tissue results, the main ROS production sources are NOX activation and mitochondrial function as both processes showed alterations 3h after AgNP incubation. These results were in line with others where the AgNP exposure positively correlated with intracellular ROS induction cytotoxicity, along with cellular antioxidant system changes through glutathione depletion and SOD and catalase induction [~~86~~79,80].

As the lung epithelial tissue is a complex multilayer system composed of several cellular types, we also decided to investigate the mechanisms underlying AgNP pulmonary toxicity in a more complex and realistic *in vitro* model, using a 3D mucociliary tissue consisting of normal, human-derived tracheal/bronchial epithelial cells that maintains the tissue morphology. Epithelial tissues are structures specialized in carrying out the primary function of a selective permeability barrier, mainly dependent on multiprotein junctional complexes. Here, we showed that airway tissue exposure to AgNP produced tissue damage and impaired barrier integrity, as indicated by TEER measurement, an electrical parameter widely used to characterize toxicant-induced epithelial disturbance [81]. It is easily conceivable that AgNP-induced barrier dysfunction may be linked to the high susceptibility of tight junctions to oxidative damage. In fact, in a condition of altered redox homeostasis, an increased generation of 4-HNE adducts, as we observed in AgNP-exposed A549 cells, can affect the function of a wide variety of biological macromolecules, including probably the tight junction [82]. Accordingly, this detrimental effect of AgNP revealed in a 3D *in vitro* system could also explain the increased proteins and cells content observed in the BAL fluids of the exposed mice.

Conclusions

While nanomaterials are currently used in a wide variety of applications ranging from electronics, foods, and cosmetics to medicine, not all toxicological aspects of their exposure on human health are always well understood. To shed light on the molecular mechanisms of AgNP toxicity on the lungs, in the current study, we conducted experiments in three different models using animals, human alveolar epithelial cells and a 3D in vitro airway tissue model. This multimodal approach enabled us to uncover new insights into the detrimental processes triggered by AgNP inhalation on the respiratory tract. The intrinsic pro-oxidant properties of the NP disturbed the O_2 metabolism. Indeed, ROS overproduction initiated by the AgNP interaction with cellular organelles such mitochondria and enzymes including NOX resulted in an impaired cellular antioxidant defense with consequent AEC oxidative damage. These harmful effects mirrored in the disruption of the alveolar-capillary barrier integrity and in an increased epithelial permeability along with cells and plasma proteins leakage into the alveolar space, which suggest an impaired lung function due to AgNP inhalation. Taken together, these findings highlight the need for regulatory measures in the nanotechnology field to limit the associated potential risks to human health.

Declarations

Ethics approval and consent to participate

All experimental animal protocols were approved by the Animals Ethics Committee of the School of Pharmacy and Biochemistry, University of Buenos Aires (Reference number 2346/18). All procedures were carried out in accordance with institutional guidelines.

Consent for publication

Not applicable.

Availability of data and material

The datasets used and/or analyzed during the current study are available from the corresponding author on reasonable request.

Competing interest

The authors declare that they have no competing interests.

Funding

This study was supported by grants from the Universidad de Buenos Aires (200201701100441BA)

References

[1] Oberdörster G, Oberdörster E, Oberdörster J. Nanotoxicology: An emerging discipline evolving from studies of ultrafine particles. *Environ Health Perspect*. 2005; 113(7): 823-39.

[2] Soares S, Sousa J, Pais A, Vitorino C. Nanomedicine: Principles, Properties, and Regulatory Issues. *Front Chem*. 2018; 2086: 360-380.

[3] Missaoui W, Arnold R, Cummings B. Toxicological status of nanoparticles: what we know and what we don't know. *Chem Biol Interact*. 2018; 295:1-12.

[4] Theodorou I, Ryan M, Tetley T, Porter A. Inhalation of silver nanomaterials-seeing the risks. *Int J Mol Sci*. 2014; 15: 23936-23974.

~~[5] Sond I, Solopek-Sondi B. Silver nanoparticle as antimicrobial agent: A case study on E-coli as a model for gram- negative bacteria. *J Colloid Interface Sci*. 2014; 275 (1): 177-82.~~

~~[6] Wei D, Sun W, Qian W, Ye Y, Ma X. The synthesis of chitosan bases silver nanoparticle an their antibacterial activity. *Carbohydr Res*. 2009. 17: 2375-82.~~

[5] Dakal T, Kumar A, Majumdar R, Yadav V. Mechanistic basis of antimicrobial actions of silver nanoparticles. *Front Microbiol*. 2016; 1831.

[6] Ferdous Z, Nemmar A. Health impact of silver nanoparticles: A review of the biodistribution and toxicity following various routes of exposure. *Int J Mol Sci*. 2020; 21(7):2375.

[7] Murdock RC, Braydich-Stolle L, Schrand AM, Schlager JJ, Hussain SM. Characterization of nanomaterial dispersion in solution prior to in vitro exposure using dynamic light scattering technique. *Toxicol Sci*. 2008; 101 (2): 239-53.

[8] Devi P, Patil SD, Jeevanandam P, Navane NK, Singla ML. Synthesis, characterization and bactericidal activity of silica/silver core-shell nanoparticle. *J Mater Sci Mater Med*. 2014; 25(5): 1267-73.

[9] Yacaman M, Ascencio J, Liu H, Gardea-Torresday J. Structure shape and stability of nanometric sized particles. J. Vacuum Sci. Technol. B. Microelectron. *Nanometer Struct*. 2001; 19: 1091-1103.

~~[12] Morones J, Elechiguerra J, Camacho A, Holt K, Kouri J, Ramirez J, ET AL. The bactericidal effect of silver nanoparticles. *Nanotechnology*. 2005; 169: 2346-2353.~~

[10] Collins T, Markus E, Hassett D, Robinson J. The effect of a cationic porphyrin on *pseudomonas aeruginosa* Biofilms. *Curr Microbiol*. 2010; 411-416.

[11] Jeong Y, Lim D.W, Choi J. Assessment of size-dependent antimicrobial and cytotoxic properties of silver nanoparticles. *Adv Mater Sci Eng*. 2014; 6.

[12] Tolaymat T.M, El Badawy A.M, Genaidy A, Scheckel K.G, Luxton T.P, Suidan M. An evidence-based environmental perspective of manufactured silver nanoparticle in syntheses and applications: A systematic review and critical appraisal of peer-reviewed scientific papers. *Sci Total Environ*. 2010; 408: 999–1006.

~~[15] Lu Z, Rong K, Li J, Yang H, Chen R. Size-dependent antibacterial activities of silver nanoparticles against oral anaerobic pathogenic bacteria. *J Mater Sci*. 2013; 24: 1465–1471.~~

[13] Benn T, Cavanagh B, Hristovski K, Posner JD, Westerhoff P. The release of nanosilver from consumer products used in the home. *J Environ Qual*. 2010; 39(6):1875-1882.

~~[18] Park J, Kwak B.K, Bae E, Lee J, Kim Y, Choi K, Yi J. Characterization of exposure to silver nanoparticles in a manufacturing facility. *J Nanopart Res*. 2009; 11: 1705–1712.~~

[14] Kuhlbusch T.A, Asbach C, Fissan H, Gohler D, Stintz M. Nanoparticle exposure at nanotechnology workplaces: A review. *Part Fibre Toxicol*. 2011; 8: 22.

[15] WHO. Guidelines on protecting workers from potential risks of manufactured nanomaterials. Geneva: World Health Organization 2017. ISBN-13:978-92-4-155004-8.

[16] Buzea C, Pacheco LL, Robbie K. Nanomaterials and nanoparticles: sources and toxicity. *Biointerphases*. 2007; 2(4): 17-71.

[17] Tetley TD. Health effects of nanomaterials. *Biochem Soc Trans*. 2007; 35 (3): 527-31.

[18] Li JJ, Muralikrishnan S, Ng CT, Yung LY, Bay BH. Nanoparticles induced pulmonary toxicity. *Exp Biol Med*. 2010; 235 (9): 1025-33.

[19] Mebert A, Aimé C, Alvarez G, Shi Y, Flor S, Lucangioli S, Desimone M, Coradin T. Silica core-shell particles for the dual delivery of gentamicin and rifamycin antiobitics. *J Mater Chem*. 2016; 4(18):3135-3144.

~~[25] Cagel M, Bernabeu E, Gonzalez L, Lagomarsino E, Zubillaga M, Moretton MA, Chiappetta DA. Mixed micelles for encapsulation of doxorubicin with enhanced in vitro cytotoxicity on breast and ovarian cancer cell lines versus Doxil®. *Biomed. Pharmacother*. 2017; 95: 894-903.~~

[20] Grotz E, Tateosian NL, Salgueiro J, Bernabeu E, Gonzalez L, Manca ML, Amiano N, Valenti D, Manconi M, García V, Moretton MA, Chiappetta DA. Pulmonary delivery of rifampicin-loaded soluplus micelles against *Mycobacterium tuberculosis*. J *Drug Deliv Sci Technol.* 2019; 53: 101170.

[21] Ale A, Bacchetta C, Rossi A.S, Galdopórpora J.M, Desimone M.F, de la Torre F.R, Gervasio S, Cazenave J. Nanosilver toxicity in gills of a neotropical fish: Metal accumulation, oxidative stress, histopathology and other physiological effects. *Ecotox Environ Safety*. 2018; 148: 976–984

[22] Chen Q, Vazquez E, Moghaddas S, Hoppel C, Lesnefsky E. Production of reactive oxygen species by mitochondria: central role of complex III. *J Biol Chem.* 2013; 278: 36027–36031.

[23] Magnani N, Marchini T, Garcés M, Mebert A, Cáceres C, Diaz L, Desimone M, Evelson P. Role of transition metals present in air particulate matter on lung oxygen metabolism. *Int J Bioch Cell Biol*. 2016; 81: 419–426.

[24] Lehman S, Morris A, Mueller P, Salem A, Grassian V, Larsen S. Silica nanoparticle-generated ROS as a predictor of cellular toxicity: mechanistic insights and safety by design. *Environ Sci Nano*. 2016; 3 (1): 56-66.

[25] Southam D, Dolovich M, O'Byrne P, Inman M. Distribution of intranasal instillations in mice: effects of volume, time, body position, and anesthesia. *Am J Physiol Lung Cell Mol Physiol*. 2002; 282: 833–839.

[26] Carvalho T, Peters J, Williams R. Influence of particle size on regional lung deposition-What evidence is there? *Int J Pharm*. 2011; 406(1-2): 1-10.

[27] Weldon B, Faustman E, Oberdörster G, Workman T, Griffith W, Kneuer C, Yu J. Occupational exposure limit for silver nanoparticles: considerations on the derivation of a general health-based value. *Nanotoxicology*. 2016; 10(7): 770-81.

[28] Wang X, Ji Z, Chang CH, Zhang H, Wang M, Liao YP, Lin S, Meng H, Li R, Sun B, Winkle LV, Pinkerton KE, Zink JI, Xia T, Nel AE. Use of Coated Silver Nanoparticles to Understand the Relationship of Particle Dissolution and Bioavailability to Cell and Lung Toxicological Potential. *Small*. 2014; 10:385–398.

[29] Seiffert J, Hussain F, Wiegman C, Li F, Bey L, Baker W, Porter A, Ryan MP, Gow A, Zhang J, Zhu J, Tetley TD, Chung KF. Pulmonary toxicity of instilled silver nanoparticles: influence of size, coating and rat strain. PLoS One. 2015; 10(3): 119726.

[30] Valacchi G, Davis PA, Khan EM, Lanir R, Maioli E, Pecorelli A, Cross CE, Goldkorn T. Cigarette smoke exposure causes changes in Scavenger Receptor B1 level and distribution in lung cells. *Int J Biochem Cell Biol*. 2011; 43(7):1065–1070.

[31] Vanasco V, Cimolai M,Evelson P, Alvarez S (2008) The oxidative stress and the mitochondrial dysfunction caused by endotoxemia are prevented by α-lipoic acid. *Free Radic Res*. 2018; 42: 815–823.

[32] Evelson E, Travacio M, Repetto M, Escobar J, Llesuy S, Lissi E. Evaluation of total reactive antioxidant potential (TRAP) of tissue homogenates and their cytosols. *Arch Biochem Biophys*. 2001; 388: 261–266.

[33] Magnani N, Marchini T, Vanasco V, Tasat D, Alvarez S, Evelson P. Reactive oxygen species produced by NADPH oxidase and mitochondrial dysfunction in lung after an acute exposure to Residual Oil Fly Ashes. *Toxicol Appl Pharmacol*. 2013; 270: 31–38.

[34] Vico T, Marchini T, Ginart S, Lorenzetti M, Areán J, Calabró V, Garcés M, Ferrero M , Mazo T, D'annunzio V, Gelpi R, Corach D, Evelson P, Vanasco V, Alvarez S. Mitochondrial bioenergetics limits inflammation and cardiac contractility in endotoxemia. *Basic Res Cardiol*. 2019; 114(5): 38.

~~[41] Poderoso J, Fernandez S, Carreras M,Tchercanski D, Acevedo C, Rubio M, Peralta J, Boveris A. Liver oxygen uptake dependence and mitochondrial function in septic rats. *Circ Shock*. 1994; 44: 175–182.~~

[35] Leung D, Chu S. Measurement of oxidative stress: mitochondrial function using the seahorse system. *Methods Mol Biol*. 2018; 1710:285-293.

~~[43] Brand MD, Nicholls DG. Assessing mitochondrial dysfunction in cells. *Biochem J*. 2011; 435: 297–312.~~

[36] Adami P, Quijano C, Magnani N, Galeano P, Evelson P, Cassina A, Do Carmo S, Leal M, Castaño E, Cuello A, Morelli L. Synaptosomal bioenergetic defects are associated with cognitive impairment in a transgenic rat model of early Alzheimer´s disease. *J Cereb Blood Flow Metab*. 2017; 37(1):69-84.

[37] Vaquero E, Edderkaoui M, Pandol S, Gukovsky I, Gukovskaya A. Reactive oxygen species produced by NAD(P)H oxidase inhibit apoptosis in pancreatic cancer cells. *J Biol Chem*. 2004; 279: 34643–34654.

[38] Cervellati F, Muresan X, Sticozzi C, Gambari R, Montagner G, Forman H, Torricelli C, Maioli E, Valacchi G. Comparative effects between electronic and

cigarette smoke in human keratinocytes and epithelial lung cells. *Toxicol In vitro*. 2014; 28(5): 999-1005.

[39] Chen L, Lippmann M. Effects of metals within ambient air particulate matter (PM) on human health. *Inhal Toxicol*. 2009; 2: 1–31.

~~[48] McCord J, Fridovich I. Superoxide dismutase. Enzymic function for erythrocuprein (hemocuprein). *J Biol Chem.* 1969; 241: 4353-4356.~~

[40] Lasagni Vitar RM, Tau J, Janezic NS, Tesone AI, Hvozda Arana AG, Reides CG, Berra A, Ferreira SM, Llesuy SF. Diesel exhaust particles (DEP) induce an early redox imbalance followed by an IL-6 mediated inflammatory response on human conjunctival epithelial cells. *Exp Eye Res*. 2018; 171:37-47.

[41] Chance, B. (1954) En *Special Methods: Catalase* (Ed. Glick, R), Interscience, New York, Estados Unidos, pp 408-424.

[42] Levine R.L, Williams J.A, Stadtman R.E, Shacter E. Carbonyl assays for determination of oxidatively modified proteins. *Methods Enzymol*. 1994; 233: 346–357.

[43] Magnani N, Muresan XM, Belmonte G, Cervellati F, Sticozzi C, Pecorelli A, Miracco C, Marchini T, Evelson P, Valacchi G. Skin Damage Mechanisms Related to Airborne Particulate Matter Exposure. *Toxicol Sci*. 2015; 149(1):227-36.

~~[51] Rodriguez-Ariza R, Toribio F, López-Barea J. Rapid determination of glutathione status in fish liver using high-performance liquid chromatography and electrochemical detection. *J Chromatogr Biomed Appl*. 1994; 656: 311–318.~~

[44] Srinivasan B, Kolli A, Esch M, Abaci H, Schuler M, Hickman J. TEER measurement techniques for *in vitro* barrier model systems. *J Lab Autom*. 2015; (20): 107-126.

[45] Lowry O, Rosebrough A, Farr A, Randall R. Protein measurement with the phenol reagent. J Biol Chem. 1951; 193: 265–275.

[46] Bradford MM. A rapid and sensitive method for the quantitation of microgram quantities of protein utilizing the principle of protein-dye binding. *Anal Biochem*. 1976; 72:248-54.

[47] Danaei M, Dehghankhold M, Ataei S, Hasanzadeh Davarani F, Javanmard R, Dokhani A, Khorasani S, Mozafari MR. Impact of particle and polydispersity index on the clinical applications of lipidic nanocarrier system. *Pharmaceutics*. 2008; 10(2).

[48] Mühlfeld C, Gehr P, Rothen-Rutishauser B. Translocation and cellular entering mechanism of nanoparticles in the respiratory tract. *Swiss Med Wkly*. 2008; 138 (27-28):387-91.

[49] Puisney C, Baeza-Squiban A. Mechanism of uptake and translocation of nanomaterial in the lung. *Adv Exp Med Biol*. 2018; 1048: 21-36.

[50] Magnani N, Marchini T, Calabró V, Alvarez S, Evelson P. Role of mitocondria in the redox signaling network and its outcomes in high impact inflammatory syndromes. *Front Endocrinol*. 2020; 11:568305.

[51] Yang L, Kuang H, Zhang W, Aguilar ZP, Wei H, Xu H. Sci Rep. 2017; 12;7(1):3303.

[52] Braakhuis HM, Park MV, Gosens I, y col. Physicochemical characteristics of nanomaterials that affect pulmonary inflammation. *Part Fibre Toxicol*. 2014; 11:18.

[53] Dayem A, Hossain M, Lee S, Kim K, Saha S, Yang G, Choi H, Cho S. The role of reactive oxygen species (ROS) in the biological activities of metallic nanoparticles. *Int J Mol Sci*. 2017; 18(1):120.

[54] AshaRani P, Low Kah Mun G, Hande M.P, Valiyaveettil S. Cytotoxicity and genotoxicity of silver nanoparticles in human cells. *ACS Nano*. 2008; 3:279–290.

~~[63] Long YM, Hu LG, Yan XT, Zhao XC, Zhou QF, Cai Y, Jiang GB. Surface ligand controls silver ion release of nanosilver and its antibacterial activity against Escherichia coli. *Int J Nanomed*. 2017; 12:3193.~~

[55] Kailasa SK, Park TJ, Rohit JV, Koduru JR. Antimicrobial activity of silver nanoparticles. *Nanoparticles in Pharmacotherapy*. 2019; 461–484.

[56] Lee SH, Jun BH. Silver nanoparticles: Synthesis and application for nanomedicine. *Int J Mol Sci*. 2019; 20:865.

[57] Nazarenko Y, Han TW, Lioy PJ, Mainelis G. Potential for exposure to engineered nanoparticles from nanotechnology-based consumer spray products. *J Expo Sci Environ*. Epidemiol. 2011; 21: 515.

[58] Lorenz C, Hagendorfer H, von Goetz N, Kaegi R, Gehrig R, Ulrich A, Scheringer M, Hungerbühler K. Nanosized aerosols from consumer sprays: Experimental analysis and exposure modeling for four commercial products. *J Nanopart Res*. 2011; 13: 3377–3391.

[59] Quadros M, Marr L. Environmental and human health risks of aerosolized silver nanoparticles. *J Air Waste Manag Assoc*. 2010; 60(7): 770-81.

[60] Mihalache R, Verbeek J, Graczyk H, Murashov V, van Broekhuizen P. Occupational exposure limits for manufactured nanomaterials, a systematic review. *Nanotoxicology*. 2017; 11:7–19.

~~[70] Zhang X, Wu H, Wu D, Wang J, Chang J, Zhai Z, Meng A, Liu P, Zhang L, Fan F. Toxicologic effects of gold nanoparticles in vivo by different administration routes. *Int J Nanomedicine*. 2010; 5:771-781.~~

[61] Bailly A, Correard F, Popov A, Tselikov G, Chaspoul F, Appay R, Al-Kattan A, Kabashin A, Braguer D, Esteve M. *In vivo* evaluation of safety, biodistribution and pharmakinetic of laser-synthesized gold nanoparticles. *Scientific Reports*. 2019; 9:12890.

[62] Detampel P, Ganguly A, Tehranian S, Green F, Singha S, Santamaria P, Jeje A, Cho C, Petri B, Amrein M. *In vivo* clearence of nanoparticles by transcytosis across alveolar epithelial cells. PLoS One. 2019;14(9): e0223339.

[63] Chen C, Wu M, Ho Y, Gung P, Tsai M, Orekhov A, Sobenin I, Lin P, Yet S. Exposure to zinc oxide nanoparticle disrupts endothelial tight and adherens junction s and induces pulmonary inflammatory cell infiltration. *Int J Mol Sci*. 2020; 21 (10): 3437.

[64] Caceres L, Paz ML, Garcés M, Calabró V, Magnani ND, Martinefski M, Martino Adami PV, Caltana L, Tasat D, Morelli L, Tripodi V, Valacchi G, Alvarez S, Gonzalez Maglio D, Marchini T, Evelson E. NADPH oxidase and mitochondria are relevant sources of superoxide anion in the oxinflammatory response of macrophages exposed to airborne particulate matter. *Ecotox Environ Safety*. 2020; 205: 111186.

[65] Kim S, Choi JE, Choi J, Chung KH, Park K, Yi J, Ryu DY. Oxidative stress-dependent toxicity of silver nanoparticles in human hepatoma cells. Toxicol In Vitro. 2009, 23(6):1076-84

[66] Andreyev A, Kushnareva K, Starkov A. Mitochondrial metabolism of reactive oxygen species. *Biochemistry (Mosc).* 2005; 70: 200–214.

[67] Xia T, Kovochich M, Nel A. Impairment of mitochondrial function by particulate matter (PM) and their toxic components: implications for PM-induced cardiovascular and lung disease. *Front Biosci*. 2007; 12:1238–1246.

[68] Marchini T, Magnani N, D'Annunzio V, Tasat D, Gelpi R, Alvarez S, Evelson P. Impaired cardiac mitochondrial function and contractile reserve following an acute exposure to environmental particulate matter. Biochim Biophys Acta 1830: 2545–2552.

[69] Hecker L, Logsdon NJ, Kurundkar D, Kurundkar A, Bernard K, Hock T, Meldrum E, Sanders YY, Thannickal VJ. Reversa lof persistent fibrosis aging by targeting NOX-4-Nrf2 redox imbalance. *Sci Transl Med*. 2014; 6(231): 231-47.

[70] Sun X, Yang Y, Shi J, Wang C, Yu Z, Zhang HJ. NOX4- and Nrf2-mediated oxidative stress induced by silver nanoparticles in vascular endothelial cells. *Appl Toxicol*. 2017; 37(12):1428-1437.

[71] Sthijns MMJPE, Thomgkam W, Albrechtc C, Hellack B, Bast A, Haenen GPMM, Schins RPF. Silver nanoparticles induced hormesis in A549 human epitelial cells. *Toxicol in vitro*. 2017; 40:223-233.

[72] Hou J, Zhao L, Tang H, He X, Ye G, Shi F, Kang M, Chen H, Li Y. Silver nanoparticles induced oxidative stress and mitochondrial injuries mediated autophagy in HC_{11} cells through Akt/AMPK/Mtor Pathway. *Biol Trace Elem Res*. 2020. doi: 10.1007/s12011-020-02212-w.

[73] Singh RP, Ramarao P. Cellular uptake, intracellular trafficking and cytotoxicity of silver nanoparticles. *Toxicol Lett*. 2012; 2013: 249-259.

[74] Vrek IV, Zuntar I, Petlevski R, Pavicic I, Dutour Sikiric M, Curlin M, Gaesster W. Comparison of in vitro toxicity of silver ions and silver nanoparticles on human hepatoma cells. *Environ Toxicol*. 2016; 31(6): 679-92.

[75] Petecchia L, Sabatini F, Varesio L, Camoirano A, Usai C, Pezzolo A, Rossi GA. Bronchial airway epithelial cell damage following exposure to cigarette smoke includes disassembly of tight junction components mediated by the extracellular signal-regulated kinase 1/2 pathway. *Chest*. 2019; 135: 1502-1512.

~~[80] Wittekindt OH, 2017. Tight junctions in pulmonary epithelia during lung inflammation. *Pflueg Arch Eur J Physiol*. 2017; 469: 135-147.~~

[76] Liu Y, Wei H, Tang J, Yuan J, Wu M, Yao C, Hosoi K, Yu S, Zhao X, Han Y, Chen G. Dysfunction of pulmonary epithelial tight junction induced by silicon dioxide nanoparticles via the ROS/ERK pathway and protein degradation. *Chemosphere*. 2020; 255: 126954.

[82] Gliga A, Skoglund S, Wallinder I, Fadeel B, KarlssonH. Size-dependent cytotoxicity of silver nanoparticles in human lung cells: the role of cellular uptake, agglomeration and Ag release. *Part Fibre Toxicol*. 2014; 11:11.

[77] Schlinkert P, Casals E, Boyler M, Tischler U, Hornig E, Tran N, Zhao J, Himly M, Riediker M, Oostingh G, Puntes V, Duschl A. The oxidative potential of differently charged silver and gold nanoparticles on three human lung epithelial cell types. *J Nanobiotechnology*. 2015; 13:1.

[78] Akter M, Rahman M, Ullah A, Saito T, Kurusaki M. A systematic review on silver nanoparticles-induced cytotoxicity: Physicochemical properties and perspectives. *J Adv Research*. 2018; 9:1-16.

[85] Gliga A, Di Bucchianico S, Lindvall J, Fadell B, Karlsson H. RNA-sequencing reveals long-term effects of silver nanoparticles on human lung cells. *Scientific Reports.* 2018; 8:6668.

[86] Han J, Gurunathan S, Jeong J, Chai Y, Know D, Park J, Kim J. Oxidative stress mediated cytotoxicity of biologically synthesized silver nanoparticles in human lung epithelial adenocarcinoma. *Nanoscale Res Lett*. 2014; 9(1): 459.

[79] Jian H, Qiu X, Li G, Li W, Yin L. Silver nanoparticles induced accumulation of reactive oxygen species and alteration of antioxidant systems in the aquatic plant Spidorela polyrhize. *Environ Toxicol Chem*. 2014; 33(6): 1398-405

[80] Xin L, Wang J, Fan G, Che B, Wu Y, Guo S, Tang J. Oxidative stress and mitochondrial injury-mediated cytotoxicity induced by silver nanoparticles in human A549 and HepG2 cells. *Environ Toxicol*. 2016; 31(12):1691-1699.

[81] Chen S, Einspanier R, Schoen J. Transepithelial electrical resistance (TEER): a functional parameter to monitor the quality of oviduct epithelial cells cultured on filter supports. *Histochem Cell Biol*. 2015; 144 (5): 509-515.

[82] Usatyuk PV, Parinandi NL, Natarajan V. Redox regulation of 4-hydroxy-2-nonenal-mediated endothelial barrier dysfunction by focal adhesion, adherens, and tight junction proteins. *J Biol Chem*. 2006; 281(46):35554-66.

Figures

Figure 1

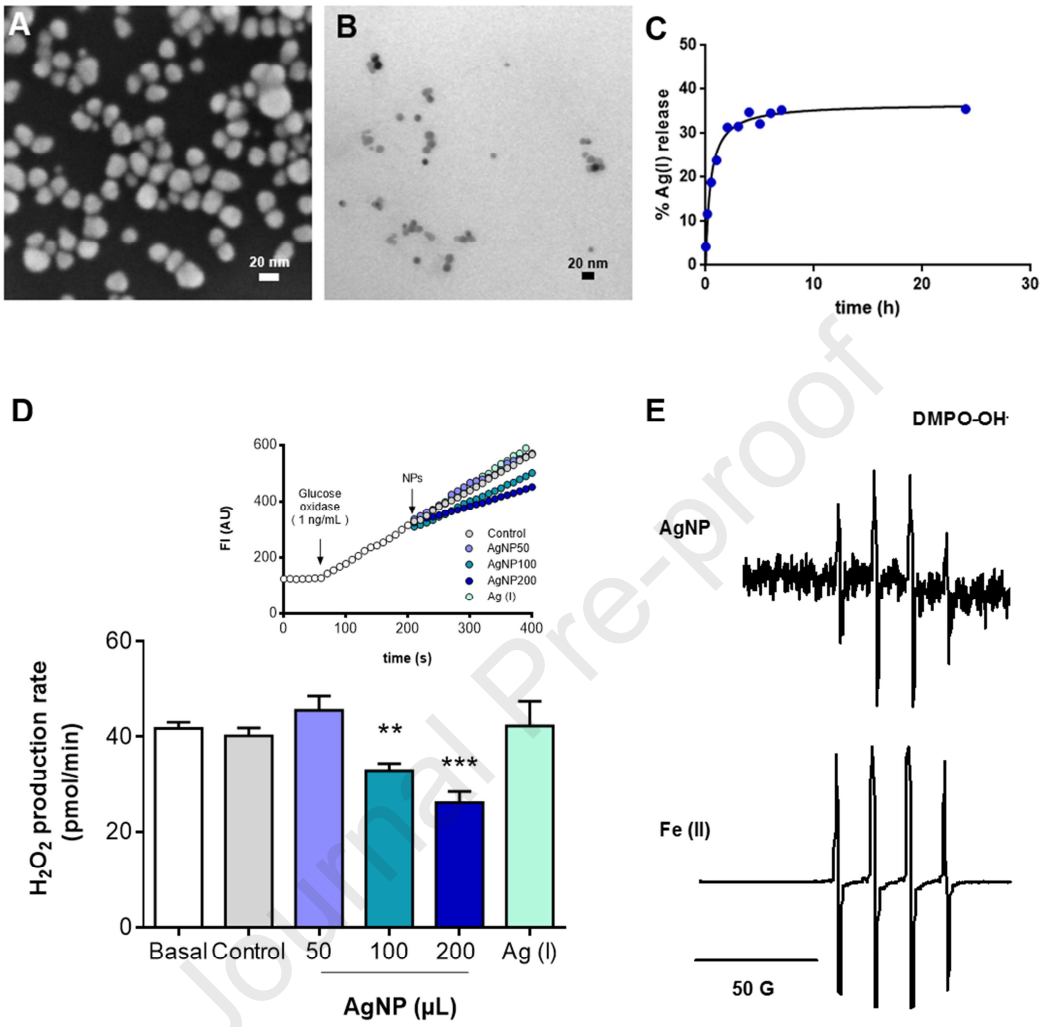

Figure 2

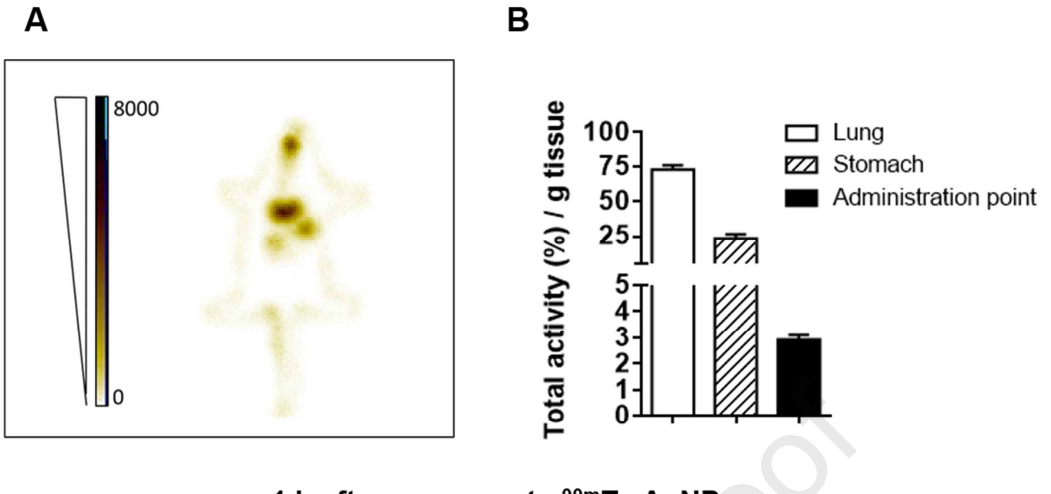

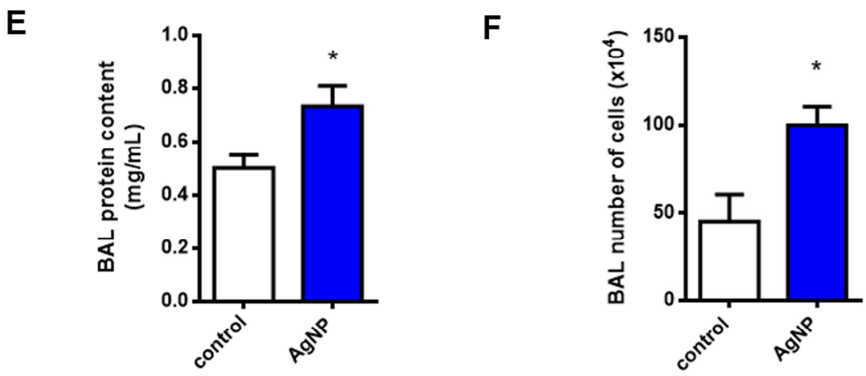

Figure 3

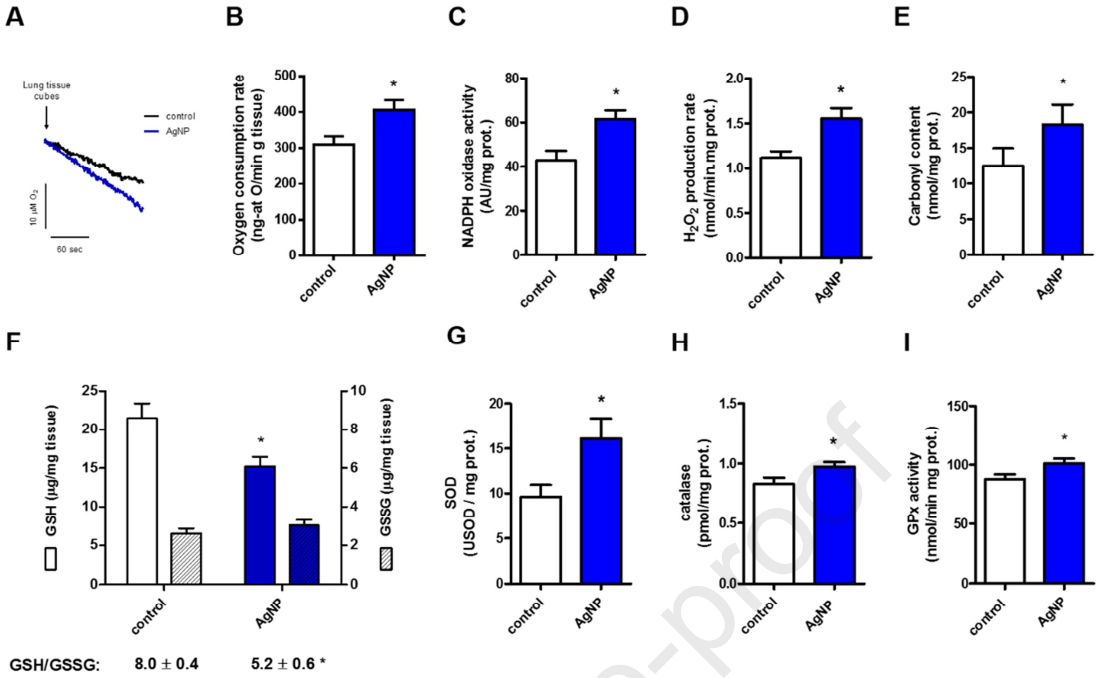

Figure 4

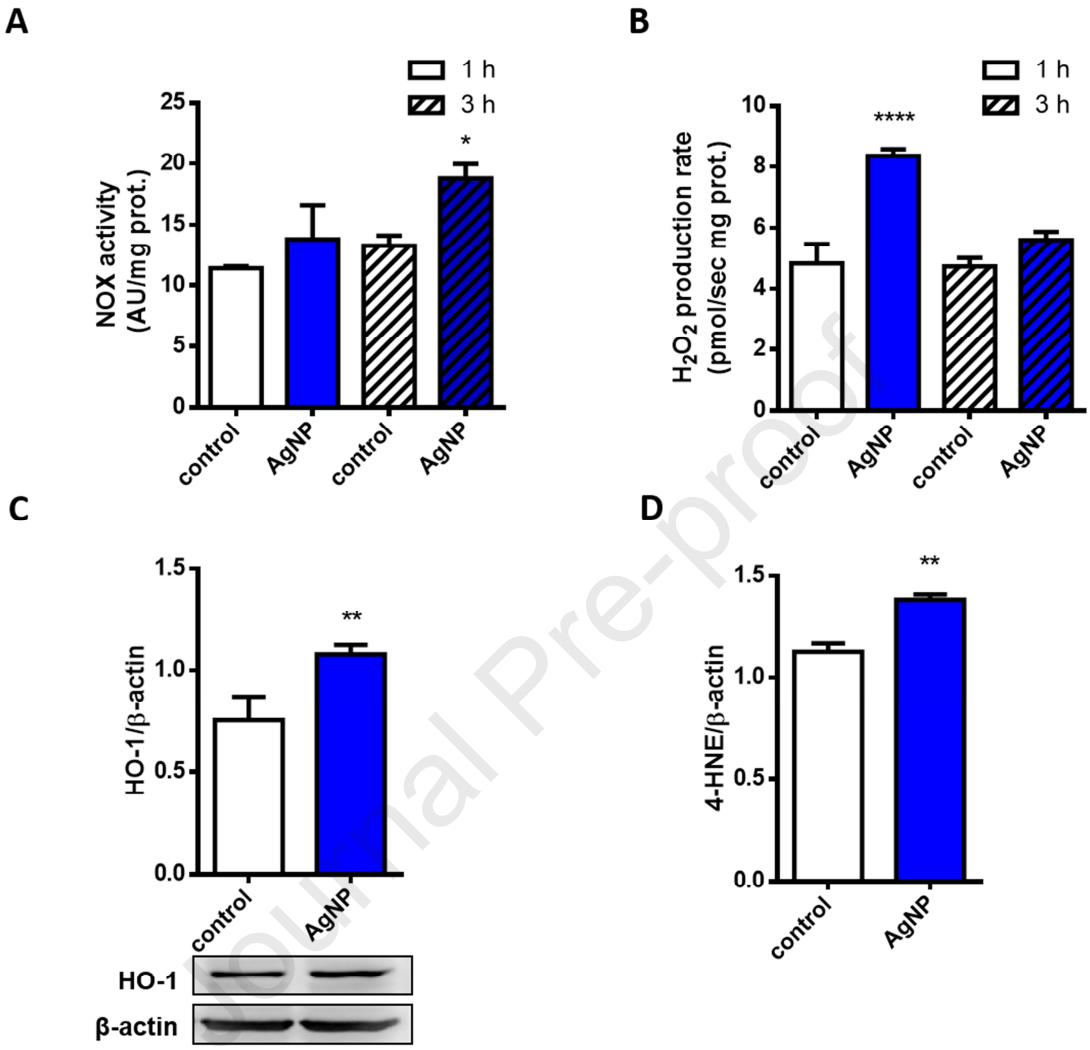

Figure 5

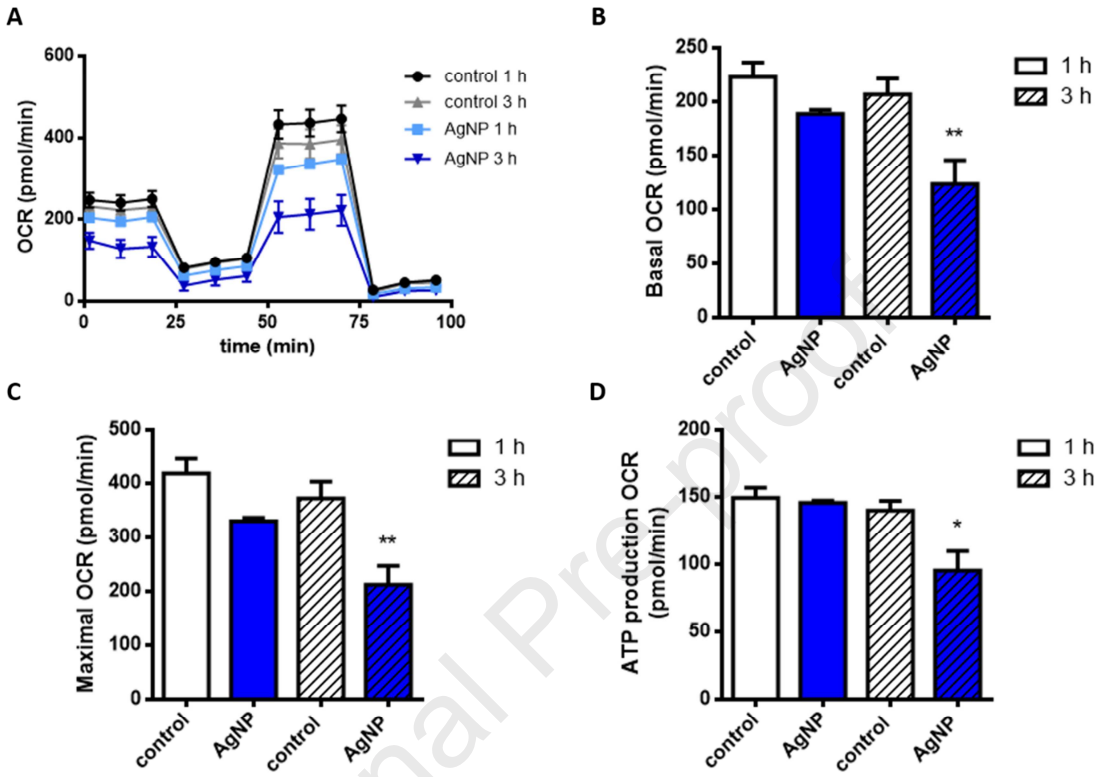

Figure 6

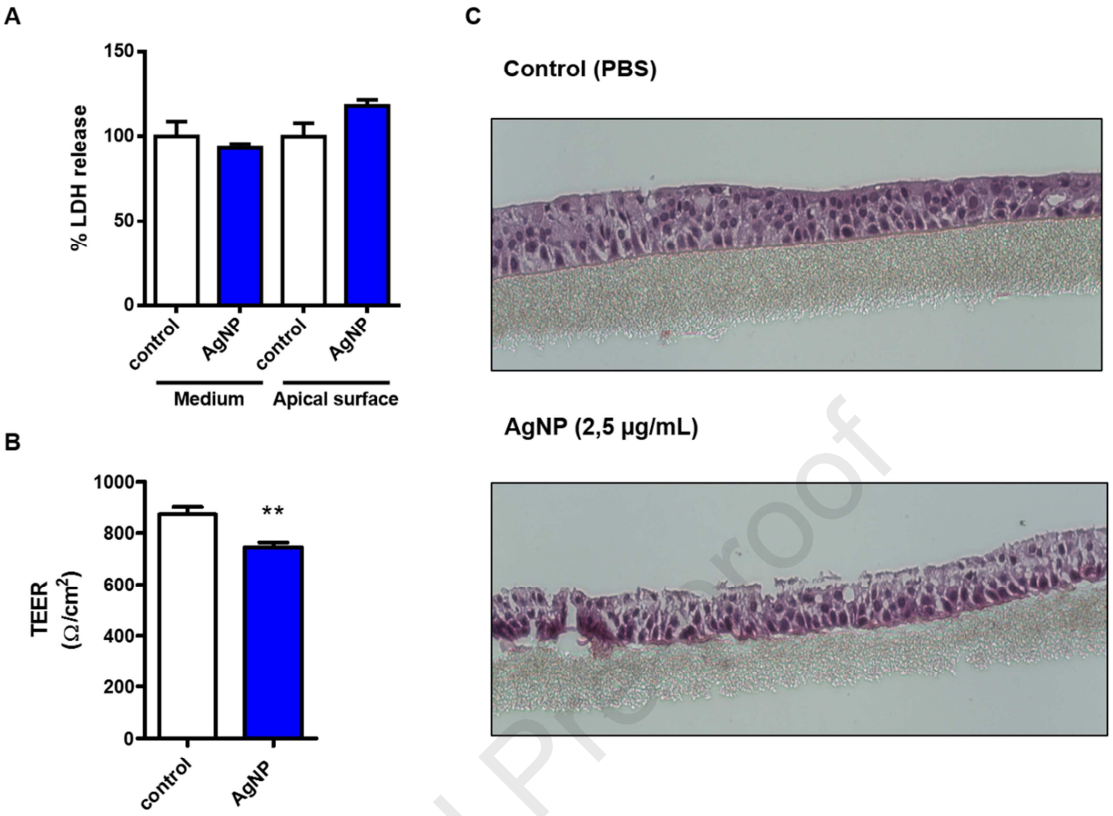

Figure S1

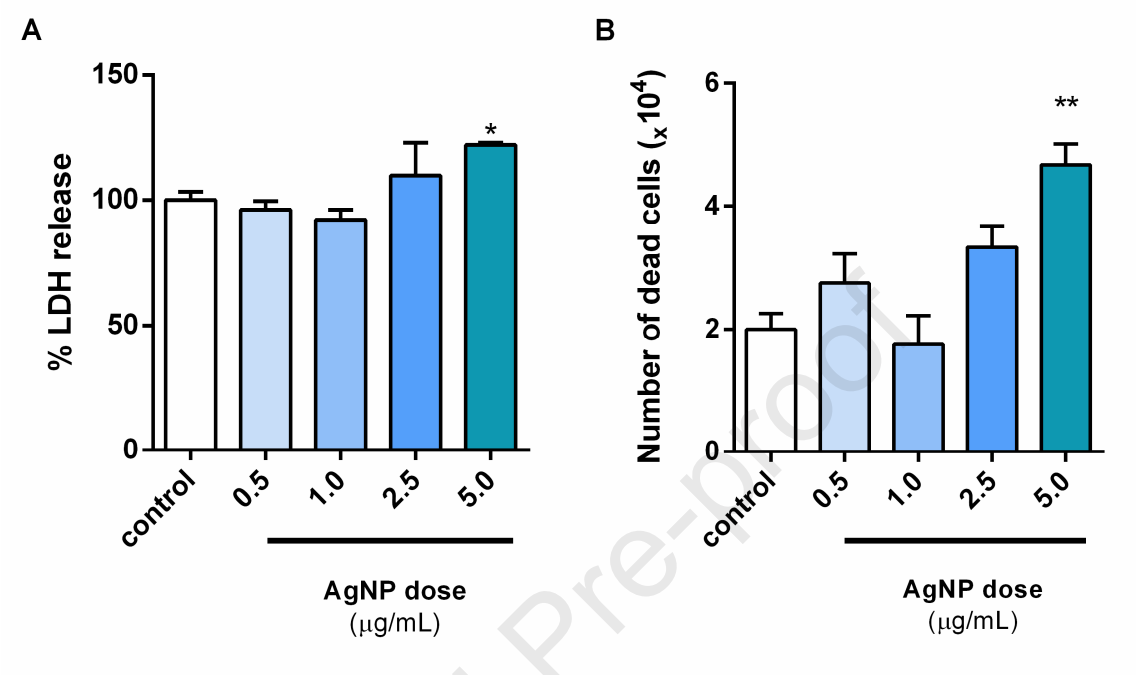

Figure legends

Figure 1: AgNP characterization and biodistribution. A) AgNP Scanning Electronic Microscopy at 500.00 K.X, scale bar 20 nm. B) NP Transmission Electron Microscopy at 400000 X, scale bar 20 nm. C) Ag(I) release from AgNP surface (0.2 mg AgNP/ mL) up to 24 h of incubation. D) Consumption of H_2O_2 generated by the glucose/glucose oxidase system using saline solution (control), AgNP (4 μg AgNP/mL), and a Ag(I) solution (4 μg Ag(I)/mL). H_2O_2 production rates were calculated from the slopes. $^{**}p<0.01$ and $^{***}p<0.001$ vs. basal H_2O_2 production rate. E) EPR spectra of hydroxyl radical ($OH^{\bullet}$) produced by AgNP (in the presence of desferrioxamine) surface-catalyzed decomposition of H_2O_2. The DMPO-$OH^{\bullet}$ spin adduct is characterized by the four-line spectrum shown of intensity 1:2:2. A solution of Fe (II) was used as positive control, since it is redox active.

Figure 2: A and C) *In vivo* static imaging by means of the acquisition of mice whole body in ventral position using gamma camera after nasal instillation with ^{99m}Tc-radiolabeled AgNP and analyzed after 1 h (A) and 24 h (C). B and D) *Ex vivo* distribution study of mice tissues as percentage of total radioactivity/g tissue after nasal instillation with ^{99m}Tc-radiolabeled AgNP and analyzed after 1 h (B) and 24 h (D). E and F) Protein content and total number of cells respectively in BAL of mice exposed to AgNP (0.1 mg/kg) after 24 h. $^{*}p<0.05$ vs. control. Data is presented as mean ± SEM, n = 6. Administration point comprises the head after removal of the brain. Imaging: 256 x 256 matrix, a 1.5 zoom, and collecting more than $1.5x10^6$ counts.

Figure 3: Lung oxidative metabolism after 1 h of exposure to saline solution or AgNP. A) Representative traces obtained during the assessment of lung O_2 consumption in 1 mm^3 tissue cubes. B) Lung O_2 consumption after the exposure to saline solution or AgNP. $^{*}p<0.05$ vs. control. C) NOX activity as lucigenin chemiluminescence after the exposure to saline solution or AgNP. $^{*}p<0.05$ vs. control. D) H_2O_2 production rate by lung isolated mitochondria after the exposure to saline solution or AgNP. $^{*}p<0.05$ vs. control. E) Protein carbonyls levels in lung homogenates. F) Lung redox balance after the exposure to saline solution or AgNP. $^{*}p<0.05$ vs. control. G-I) Activity of the antioxidant enzymes superoxide dismutase (G), catalase (H) and GPx (I) in lung homogenates. $^{*}p<0.05$ vs. control. Results are expressed as mean ± SEM of at least 6 animals per group.

Figure 4: A) NOX activity in samples of A549 cells as lucigenin chemiluminescence after 1 and 3 h of exposure to DMEM or AgNP. *p<0.001 vs. the corresponding control group. B) H_2O_2 production rate by A549 cells after 1 and 3 h of the exposure to DMEM or AgNP. ***p<0.001 vs. the corresponding control group. C) Western blot analysis of A549 cells after 1 h of exposure to DMEM or AgNP using HO-1 antibody and actin antibody as loading control (upper panel). Densitometry units ratio between HO-1 and actin (lower panel). **p<0.01 vs. control. D) Western blot quantification analysis of samples of A549 cells using anti- 4-hydroxynonenal (4-HNE) and anti-actin as loading control after 1 h of the exposure to DMEM or AgNP. **p<0.01 vs. control. Results were expressed as mean value ± SEM and represent the mean of triplicate determinations obtained in 4 separate experiments.

Figure 5: A) Representative profile trace of the oxygen consumption rate (OCR) for A549 cells. OCR was determined in the presence of pyruvate, glutamine, and glucose. Basal OCR (B), maximum OCR after the addition of 1 µM FCCP (C) and OCR associated with ATP production (D). *p<0.05, **p<0.01 vs. the corresponding control group. Results were expressed as mean value ± SEM and represent the mean of triplicate determinations obtained in 4 separate experiments.

Figure 6: A) Cytotoxicity evaluation by lactate dehydrogenase (LDH) release maintenance media and in apical washes of a 3D mucociliary tissue model consisting of normal human-derived bronchial epithelial cells (EpiAirway). B) Evaluation of the tissue integrity by measuring transepithelial electrical resistance (TEER) in EpiAirway tissue. **p<0.05. vs control. C) EpiAirway tissue morphology evaluation by hematoxilin-eosin staining. Results were expressed as mean value ± SEM and represent the mean of triplicate determinations obtained in 4 separate experiments.

Supplementary figure legend

Figure S1: Cytotoxicity evaluation by lactate dehydrogenase (LDH) release in the maintenance media (DMEM) (A) and number of A549 dead cells (B) after 24 h of exposure using 0.5, 1.0, 2.5 and 5.0 µg/mL of AgNP suspension.

Table 1: Oxygen consumption and respiratory control of mitochondria isolated from lung of mice exposed to AgNP. *p<0.05 vs. control. Data is presented as mean ± SEM, n = 6.

	control	**AgNP**
State 3 (ng-at O/min mg prot.)	28.0 ± 1.5	44.0 ± 2.4 *
State 4 (ng-at O/min mg prot.)	6.9 ± 0.7	5.0 ± 0.8
RCR	4.1 ± 0.6	8.8 ± 0.7 *

Table 2: Mitochondrial respiratory complex activity from lung of mice exposed to AgNP.**p<0.01 vs. control. Data is presented as mean ± SEM, n = 6.

	control	**AgNP**
Complexes I-III (nmol/min mg prot.)	154 ± 5	196 ± 11 **
Complexes II-III (nmol/min mg prot.)	17 ± 1	17 ± 2
Complex IV (k'10^{-2}/min mg prot.)	9 ± 1	10 ± 2

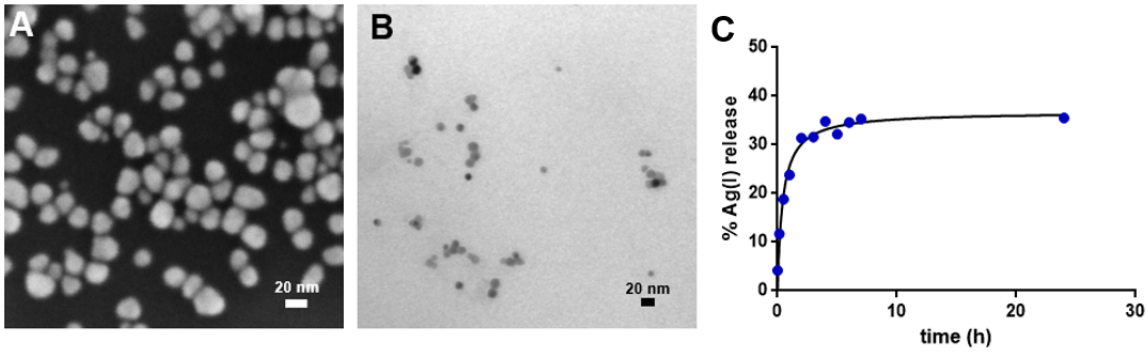

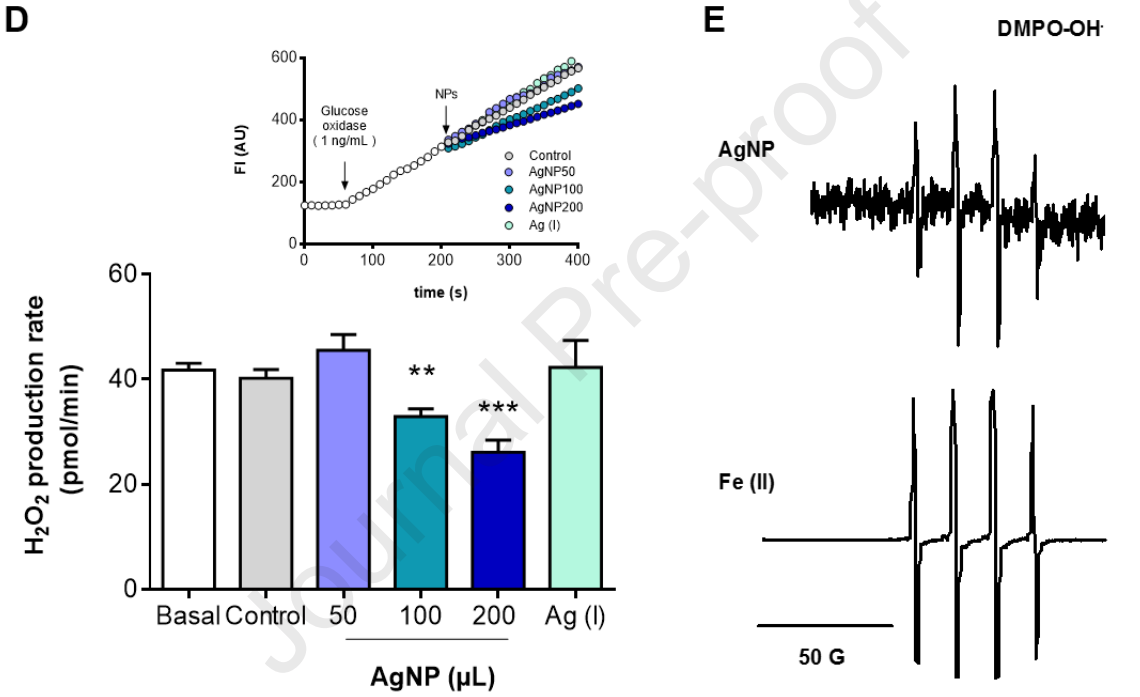

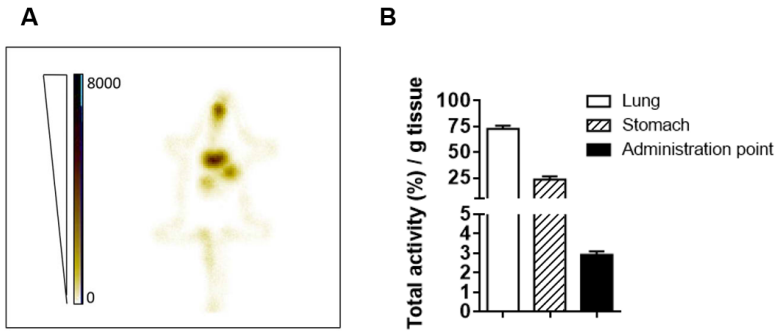

1 h after exposure to ^{99m}Tc-AgNP

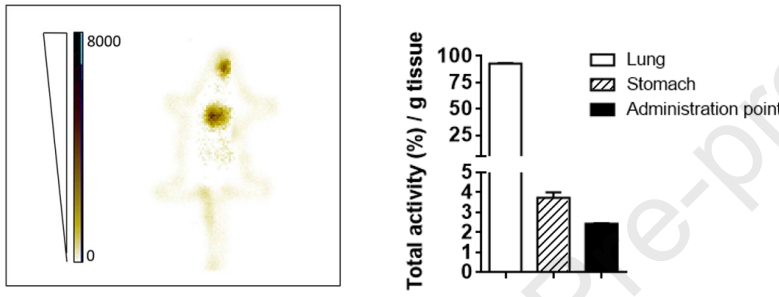

24 h after exposure to ^{99m}Tc-AgNP

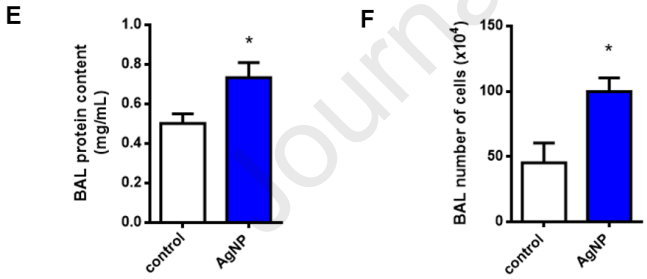

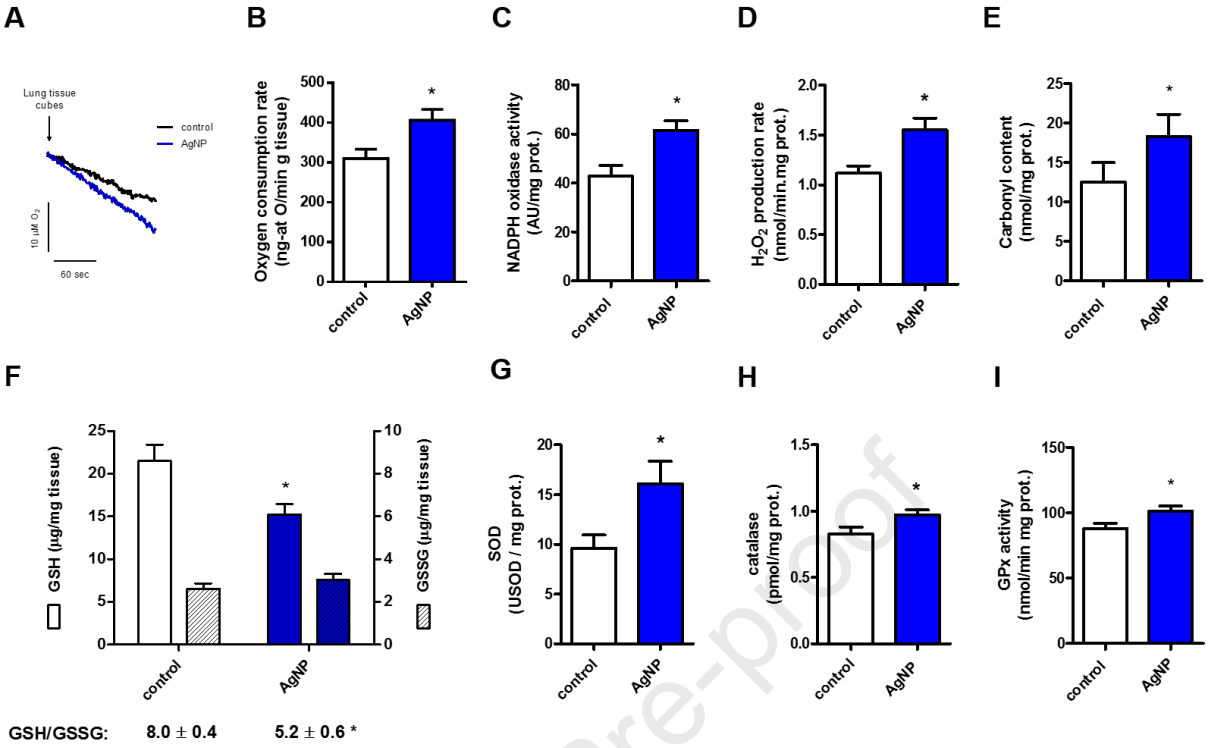

GSH/GSSG: 8.0 ± 0.4 5.2 ± 0.6 *

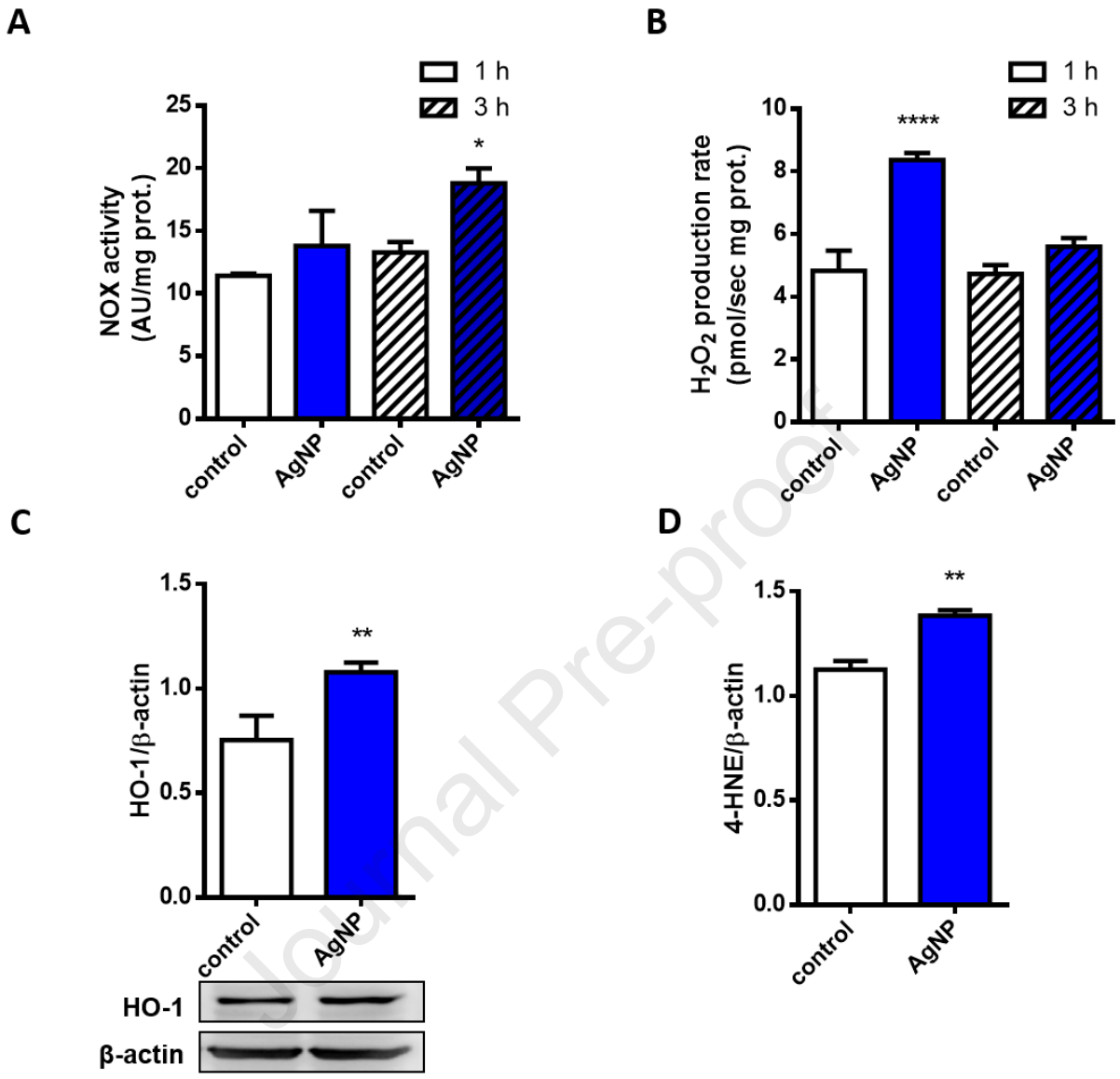

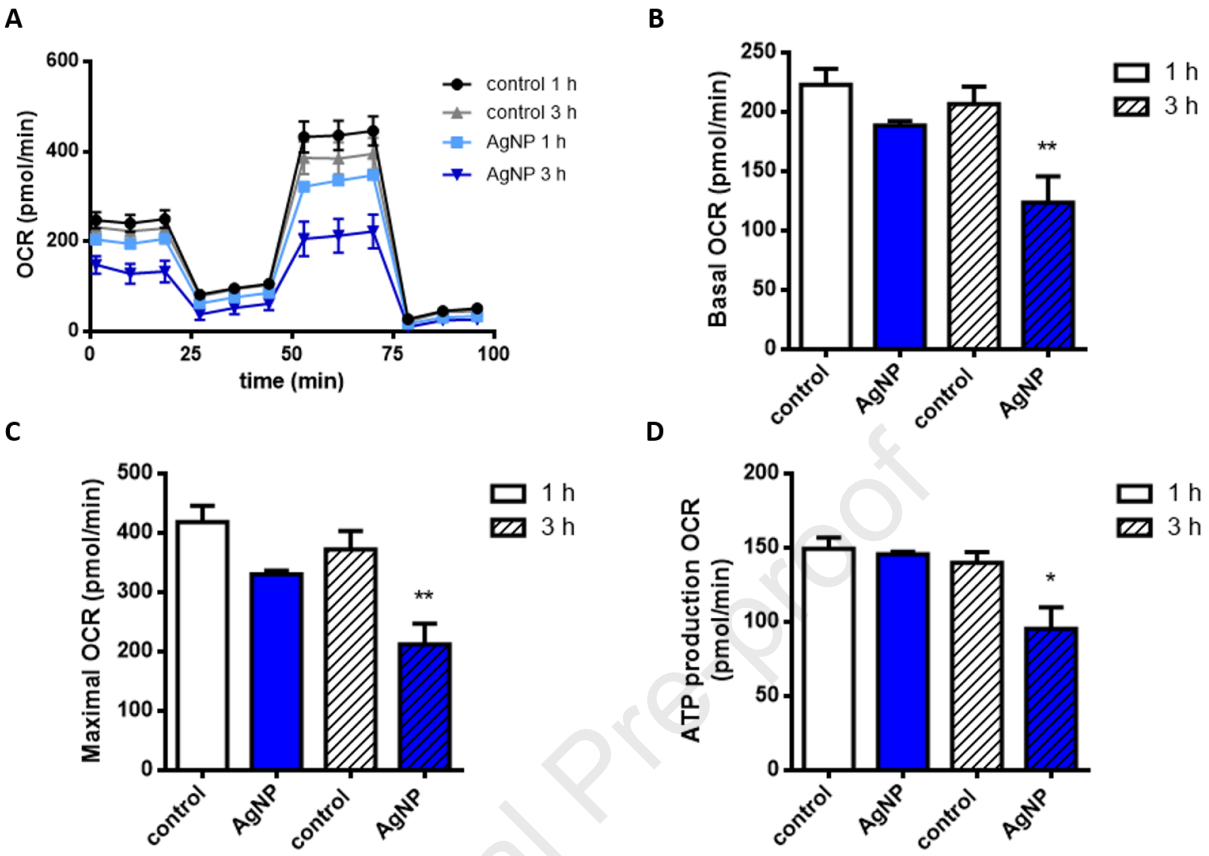

A

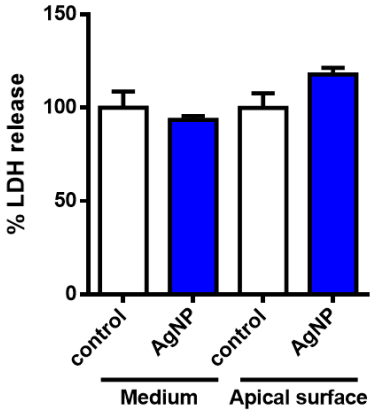

B

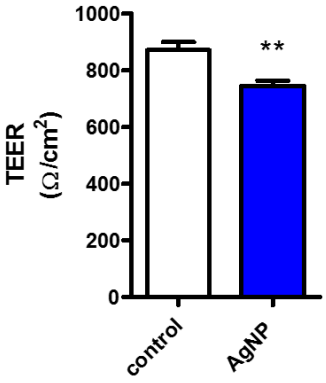

C

Control (PBS)

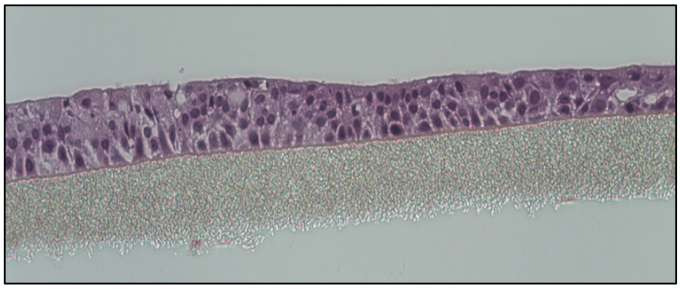

AgNP (2,5 µg/mL)

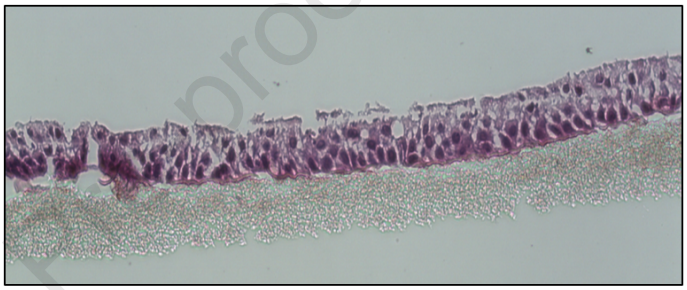

Highlights

- Exposure to AgNP altered lung tissue O_2 consumption due to increased mitochondrial active respiration and NOX activity.
- Increased NOX activity and mitochondrial H_2O_2 production rate led to oxidative damage.
- Lung 3D tissue model showed AgNP-initiated barrier alterations as TEER values decreased.
- Oxidative damage may be responsible for the impaired lung function observed due to alveolar epithelial injury.